TECHNISCHE UNIVERSITÄT WIEN
Vienna | Austria

DIPLOMARBEIT

Single molecule studies of initial T-cell activation

Ausgeführt am Institut für
Angewandte Physik
der Technischen Universität Wien

Unter der Anleitung von
UNIV. PROF. DIPL.-ING. DR. TECHN. GERHARD SCHÜTZ und
UNIV. ASS. DIPL.-ING. DR. TECHN. MARIO BRAMESHUBER

durch

DANIELA BOVENKAMP

Leopoldine-Schlinger-Gasse 2/19, 1020 Wien

October 31, 2016

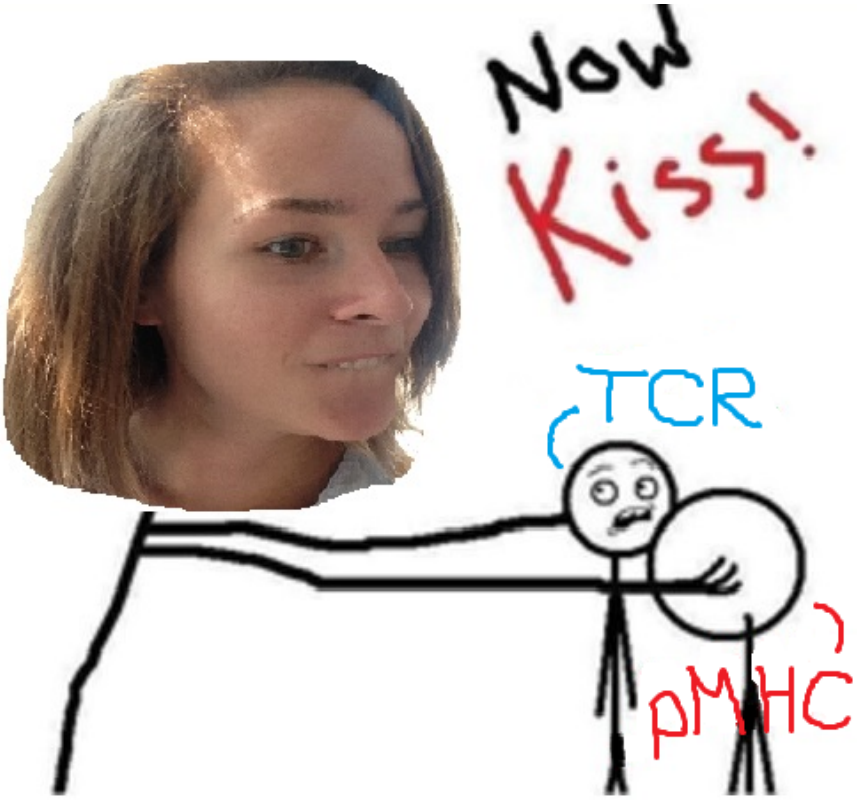

Daniela Bovenkamp

TECHNISCHE UNIVERSITÄT WIEN

Abstract

Fakultät für Physik

Angewandte Physik

Single molecule studies of initial T-cell activation

by Daniela BOVENKAMP

CD4+ T lymphocytes are capable of detecting low amounts of pathogenic peptides presented by antigen presenting cells (APC). The initial T cell activation upon successful recognition goes along with large structural changes and internal Calcium signaling. The crucial protein complex in the discrimination between different self and pathogenic peptides is the T cell receptor (TCR). It binds to its counterpart on the antigen presenting cell (APC), the peptide carrying major histocompatibility complex (pMHC). Binding dynamics between TCR and pMHC are highly debated in the immunological community. The main goal of this master thesis was to probe the interaction of the TCR with the pMHC on a single molecule level, with the latter being embedded in a synthetic lipid bilayer membrane. To this end, dwell times of single molecule Förster resonance energy transfer (smFRET) events, times of immobilizations and diffusion constants of various pMHCs under activating and non-activating conditions were determined. By comparing smFRET with immobilisation data, it was possible to show, that the direct TCR-pMHC interaction lasts shorter than the corresponding immobilization time. Furthermore, diffusion constants of various pMHC variants and a fluorescently labeled cholesterol-analogue under and adjacent to the T cell synapse were compared with each other. Thereby, it was feasible to demonstrate, that molecules in the interface of the T cell and the synthetic antigen presenting cell (APC) not only immobilized but in addition exhibited a reduced diffusion constant. Diffusion constants of pMHCs under activating and non-activating conditions - realized by a high versus a very low density of pMHC molecules - were compared, which also revealed differences in the diffusion performance. Taken together, presented studies allowed for a deeper insight in the interaction of the TCR with the pMHC.

TECHNISCHE UNIVERSITÄT WIEN

Kurzfassung

Fakultät für Physik

Angewandte Physik

Einzelmolekulare Untersuchungen von T-Zell Aktivierung

von Daniela BOVENKAMP

CD 4+ T Lymphozyten sind in der Lage, geringste Mengen an pathogenen Peptiden, die von speziellen Antigen-präsentierenden Zellen (APC) präsentiert werden, zu erkennen. Nach der erfolgreichen Erkennung des krankhaften Peptids folgt die Initialisierung der T Zell Aktivierung, welche mit großen strukturellen Veränderungen und Calzium Ausschüttung einhergeht. Den wichtigsten Proteinkomplex stellt der T Zell Rezeptor (TCR) dar, da er für die Unterscheidung zwischen ungefährlichen und krankhaften Peptiden verantwortlich ist. Der T Zell Rezeptor bindet an das Peptid, das im *peptide major histocompatibility complex* (pMHC) an der Oberfläche der APC präsentiert wird. Diese Interaktion zwischen TCR und pMHC ist aktueller Gegenstand kontroversieller Diskussionen in der Immunologie. Das Ziel dieser Diplomarbeit war ein tieferes Verständnis der Interaktion zwischen TCR und pMHC auf Einzelmolekülniveau zu erlangen. Dabei wurden Erkenntnisse über die Interaktion von einzelnen pMHC mit TCR mittels *single molecule Förster resonance energy transfer* (smFRET) Ereignissen, Immobilisierungen und Diffusionskonstanten von verschiedenen Peptiden im pMHC Komplex unter aktivierenden und nicht-aktivierenden Bedingungen gewonnen. Die Korrelation zwischen smFRET und Immobilisierungen konnte zeigen, dass die direkte Interaktion von pMHC und TCR kürzer ist, als die dazugehörige Immobilisierung. Darüberhinaus wurden Diffusionskonstanten von verschiedenen Peptiden im pMHC Komplex und einem fluoreszenzmarkierten Cholesterol als Negativkontrolle unter und neben der T Zelle gemessen und verglichen. Hierbei wurde demonstriert, dass die Moleküle unterhalb der T Zelle nicht nur langsamer diffundieren, sondern auch immobilisiert werden - im Gegensatz zu Molekülen neben der T Zelle. Mit dieser Arbeit konnten weitere Einblicke in die Interaktion von T Zell Rezeptor mit pMHC gewonnen werden.

Acknowledgements

My deepest appreciation go to Mario Brameshuber, who was always there to answer the most unnecessary and repetitively asked questions, Martin Fölser, my dearest neighbor in the office, and Lukas Schrangl, without whose help in python the programming would have been a lot more complicated.

I would also like to thank all the others in the lab, who were always available to help and support me.

A special thanks goes to Gerhard Schütz for giving me the opportunity to do my Master's thesis in his lab.

Last but definitely not least, I highly appreciate the support of my parents, Helene and Ron Bovenkamp, without whose encouragement and aid my entire academic studies would not have been possible, and my sister, Evelyn Bovenkamp, the best sister ever.

Contents

Chapter 1

Introduction

The interaction dynamics between the T cell receptor (TCR) and a peptide major histocompatibility complex (pMHC) are still an unresolved issue in immunology [26]. The correct immune response by T lymphocytes depends on the appropriate signal induction and interpretation upon pMHC recognition [8], the latter being the major objective in this thesis.

1.1 Immunology

Immunology is a very widespread field, therefore, only the most important aspects for this thesis are presented and discussed. Most of the introduction into immunology was taken from Murphy [34] and William [42].

1.1.1 The immune system

The four main functions of the immune system include the detection and elimination of harmful pathogens, regulation of appropriate immune response and generation of an immunological memory [34].

Both, lymphocytes of the innate and the adaptive immune system are responsible of recognizing infections. Therefore, the immune system consists of a broad variety of cells, which build up defense mechanisms. Rejection of tumors, elimination of many mircobial agents or tolerance of self-antigens require appropriate immune responses. If the immune system is dysregulated, autoimmune diseases are the consequence. To protect an organism against reintroduction of a pathogen, the adaptive immune system is capable of generating an immunological memory. After exposure to a pathogen, an organism will have a faster and stronger response to a subsequent exposure [34] [42].

The innate immune system responds rapidly to exposure to an infectious agent, whereas it takes some time, hours to days, for the adaptive immune

system to react to a pathogenic stimulus. However, the adaptive immune system eliminates infected organisms more efficiently due to the specificity of the antigen receptors of lymphocytes. The high amount of lymphocytes present in the body allow for a broad repertoire of antigen receptors to recognize a pathogen and induce an appropriate immune response [34].

Cells of the adaptive immune system exhibit a specific recognition of foreign antigens and, thereby, mobilizing the elimination of microbes expressing and presenting these antigens [34].

The immune response of the cells of the adaptive immune system depends on the cues from the innate immune system. The cells of the innate immune system influence the behavior of the cells of the adaptive immune system in such a way, that they control the appropriate type of response [34].

1.1.2 The cells of the immune system

Several distinct cell types compose the immmune system. Each of these cell types have important tasks to maintain the function of the immune system and induce proper immune responses to harmful pathogens. The most important cells of the immune system for this thesis are the T lymphocytes, which cover a wide range of immunologic functions [42].

The cells of the immune system are mainly present in peripheral organized tissue like spleen, lymph nodes, intestine or tonsils [34].

B- and T-Lymphocytes

Lymphocytes determine the specificity of immunity by controlling and influencing effector cells of the immune system. Cells, which interact with lymphocytes, are, for example, dendritic cells (DCs), macrophages, natural killer cells (NK cells), neutrophils, mast cells, basophils or eosinophils, which are described in the next section. The outcome of these interactions is the mediation of immunologic functions upon presentation of antigens [34].

To guide immunocompetent cells to sites, where they are required, lymphocytes circle through the blood and lymphatic system. Activated lymphocytes are not limited to the blood and lymphatic stream, they are capable of entering nonlymphoid tissues, where they induce effector functions and eliminate local infections and harmful pathogens. Memory lymphocytes are constantly checking reintroduction of their specific antigens by circling around the blood and lymphatic system [42], [34].

The development of the lymphocytes occur in the thymus and bone marrow. The name of the T-lymphocytes emerges from this aspect: Thymus-derived lymphocytes - T-Lymphocytes [34].

Individual lymphocytes express specialized sets of receptors. These receptors can only recognize a limited number of antigens, which are structurally related. Hence, for each antigen, a specfic lymphocyte exists.

Two different classes of lymphocytes exist: B-lymphocytes and T-lymphocytes. The difference between the two lymphocytes is their function [34].

- *B-Lymphocytes* are precursors of antibody secreting cells.
- *T-Lymphocytes* express their important role for the immune regulation in helper functions as they have the ability to influence the development of specific types of immune responses: production of antibodies by B-cells, increase of microbicidal activity of macrophages or the recruitment of granulocytes to sites of infection. Regulatory T cells have the ability to suppress immune response.

T-Lymphocytes are further subdivided into 2 distinct classes based on their cell surface receptor. The majority of T lymphocytes express T cell receptors consisting of α and β chains, moreover, T cells, which express TCRs with γ and δ chains, have also been found. The T lymphocytes with the α and β chains consisting TCRs can be further subdivided into two groups, based on their coreceptor, they express: CD4+ T cells express the coreceptor CD4 and CD8+ T cells have the coreceptor CD8 on their cell surface. The main difference comprises in the way they recognize antigens. CD8+ T-lymphocytes are specialized in detecting class I pMHC complexes, whereas CD4+ T cells have receptors for class II pMHC [34].

CD4+ T Lymphocytes are the major helper cells of the immune system and mediate important effector functions. Their helper functions depend on their expressed cell surface molecules (e.g. CD154) and a broad range of cytokines, which are secreted upon stimulation. Cytokines are powerful molecules, which can be directly toxic to target cells and can mobilize potent inflammatory mechanisms. Depending on the type of the secreted cytokines, a further differentiation of the CD4+ T lymphocytes is initiated. Examples for further differentiated CD4+ T cells are listed in the following [34]:

- T_{H1} cells induce cellular responses and are involved in enhancement of the microbicidal activity of monocytes and macrophages.
- T_{H2} cells are responsible for defending helminthic parasites.

- T_{H17} cells recruite efficiently granulocytes and other cells of the inflammatory sytem. They are important for responses to extracellular bacterial pathogens.
- T_{fh} cells are follicular helper cells. CD4+ T lymphocytes can differeniate to cells, which have the ability to enter B-cell follicles and, thereby, help B-cells develop into antibody-producing cells by undergoing immunoglobulin class switching and affinity maturation.

Effector cells of the immune system

Effector cells of the immune system mediate several important pathways in the immune system. Therefore, different cells have various responsibilities in controlling pathogenic tissues [42], [34].

- *Monocytes and macrophages* are responsible for eliminating organisms, which have been detected as pathogenic due to intracellular infections. Moreover, macrophages can act as antigen presenting cells (APC) by expressing pathogenic peptides, which can be recognized by CD4+ T cells, if the TCR has suitable properties. However, APC imitating macrophages do not activate naive T cells as efficiently as convenient APCs. Usually, antigens from phagocytosed infectious agents are transferred to dendritic cells, which would be the principal APCs for activating of naive or resting memory CD4+ T cells. T cells, which are activated in this way, would be available to help infected macrophages.
- *Dendritic cells (DCs)* take up antigen in peripheral sites and present antigen.
- *Natural killer cells (NK cells)* are closely related to T lymphocytes, but lack a T cell receptor. Instead, they express 2 classes of receptors, which allow for recognition of virally infected cells or tumor cells. Moreover, NK cells have receptors for MHC of cells, which are infected in a way that they cannot be recognized by cytotoxic T cells due to downregulation or depletion of expression of pMHC molecules. These cells are possible targets for NK cells.
- *Mast cells and Basophils* are important for induction of allergic inflammatory responses by releasing granules containing histamine and active agents.
- *Granulocytes* are critical for inflammatory issues.
- *Eosinophils* are required to provide proper immune response to helminths and for tissue damages, e.g. allergic inflammation reactions as in asthma. Furthermore, they kill antibody-coated parasites.

- *Neutrophils* phagocytose and activate bactericidal mechanisms.

1.1.3 Antigen recognition

One of the main differences between B- and T- lymphocytes is the mechanism of antigen recognition [34].

B-Lymphocyte

Immunoglobulin (Ig), the B-cells receptor, binds to individual antigenic epitopes, which are expressed on the surface of native molecules found on cell surface or in solution. Antibody and B-cell receptors evolved to bind and protect against microorganisms in extracellular fluids [34].

T-Lymphocyte

T-cells recognize cell-associated molecules and control their functions by interacting with and altering the behavior of APCs. The TCR is not capable of detecting antigenic structures on intact, undenatured molecules, it only recognizes complexes consisting of a peptide, which is derived by intracellular proteolysis of the antigen and embedded into a specialized scaffold complex, the pMHC [7]. MHC complexes are further subdivided into 2 classes: class I pMHC and class II pMHC. Each class of pMHC is recognized by a certain type of T-cell. CD4+ T-lymphocytes are responsible to properly detect pMHC class II molecules, on the contrary, CD8+ T-cells are required to detect pMHC class I complexes. The pMHC complexes are expressed on the cell surface and are presented to the respective type of T-lymphocyte to bind and induce the required immune responses [34].

1.2 The immunological synapse

1.2.1 Microclusters

Upon ligation of the TCR to pMHC, a special kind of aggregation of the molecules is triggered, the so called 'microclusters' (MCs) [13] [40]. Microclusters are the first functionalized complexes of TCR that can be observed at the interface of a T lymphocyte with a supported lipid bilayer, which mimics antigen presenting cells, or in cell-cell contact. These submicron structures contain 10-100 individual TCRs and are only present if the T lymphocyte is exposed to a high number of pMHCs (100 molecules/μm^2)

[39]. Ligand-induced MCs engage the kinase Lck, which is a member of the Src family, with the TCR, which causes the phosphorylation of ITAMs and recruitment and activation of zeta-chain associated protein of the size of 70kDa, ZAP70 [45]. After the formation of these MCs, the T cell arranges various molecules, adhesion proteins, costimulatory factors and the TCR bound to pMHC, in a special structure: the immunological synapse (IS). Hence, in the IS the organisation of the molecules is critical for the correct immune response of the T cell [21]. The antigen recognition itself takes place at the closest contact, which is a 15 nm gap between the T lymphocyte and the antigen presenting cell, termed the 'close contact zone' [9].

1.2.2 Supramolecular activation clusters (SMAC)

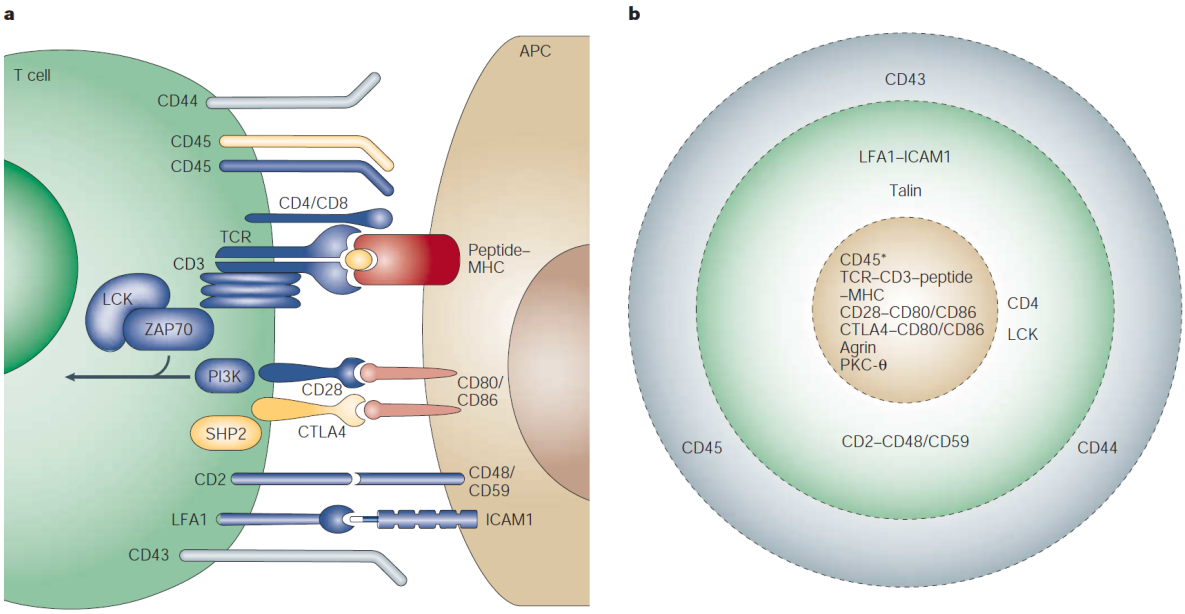

FIGURE 1.1: **Arrangement of molecules in the supramolecular activation cluster (SMAC):** Upon ligation of the T cell with an antigen presenting cell, the involved molecules are arranged in a special, ring-like formation, the supramolecular activation cluster (SMAC). *dSMAC:* The most distal ring, colored in grey in [b], includes CD45. *pSMAC:* The adjacent, proximal, ring to the cSMAC comprises ICAM-1, here highlighted in green in [b]. *cSMAC:* The most central part, colored in brown in [b], can be subdivided into two compartments: *endo-cSMAC:* the central structures of the immunological synapse, where pMHC is organized and *exo-cSMAC:* the other central structure, where TCR-enriched vesicles are released [10]. This figure is taken from Huppa and Davis [23].

The immunological synapse can be divided into different rings, depending on the presence of different molecules [14] (figure 1.1). The T cell drags and merges the MCs centripetally into the central circle, which is termed the

central supramolecular activation cluster (cSMAC) [17]. The cSMAC is surrounded by a ring of ICAM-LFA-1 molecules, which compose the peripheral supramolecular activation cluster (pSMAC). The distal supramolecular activation cluster (dSMAC) encircles the cSMAC and the pSMAC and represents the most outer ring of the SMAC complex.

dSMAC

During the formation of microclusters, transmembrane tyrosine phosphatase CD45 is removed from the TCR:pMHC interaction zones due to its large extracellular domain [14]. The exclusion of CD45 seems to be important for the phosphatase activity in TCR triggering [9] [13]. Hence, CD45 is accumulated in the distal ring of the supramolecular cluster. The dSMAC can be compared to the leading lamellipodium of migrating cells ever since it repeates cycles of protrusion and retraction.

pSMAC

The pSMAC is primarily composed of LFA-1, the counterpart of ICAM-1, which is responsible for adhesion [15].

cSMAC

Recently, it has been observed that the cSMAC not only consists of TCR-pMHC ligations but can moreover be subdivided into two zones: the endo and the exo cSMAC [14]. In the endo cSMAC, TCR and CD28 maintain signalling in the synapse. Whereas the exo cSMAC is the site of TCR-enriched extracellular vesicles, termed as 'ectosomes' [10]. These ectosomes are of special importance for the interaction of T cells with B cells: The B cells remove the ectosome by endocytosis of the TCR-enriched vesicles from the interface. Furthermore, CD28-CD80 interactions are separated from the TCR bulk. CD80, or B7-1, belongs to the group of costimulatory molecules.

1.2.3 Receptors of the immunological synapse

Even though, there are numerous receptors in the immunological synapse present, only the most important ones beside the TCR are briefly described in the following. For this thesis, pMHC, ICAM-1 and B7-1 were the molecules of interest on the side of the APC, which is mimicked by a supported lipid bilayer system (see chapter 3, *Characterization of the APC mimicking supported lipid bilayer*).

pMHC

Figure 1.2 shows the structure of the ligation of TCR:pMHC. In this complex a peptide is presented to the TCR resulting in a binding and induction of the required immune response [27] [26] [22]. pMHC complexes are produced inside of antigen presenting cells (APCs). pMHC class I peptides are derived from internally synthesized proteins, whereas, pMHC class II peptides originate from imported proteins [34].

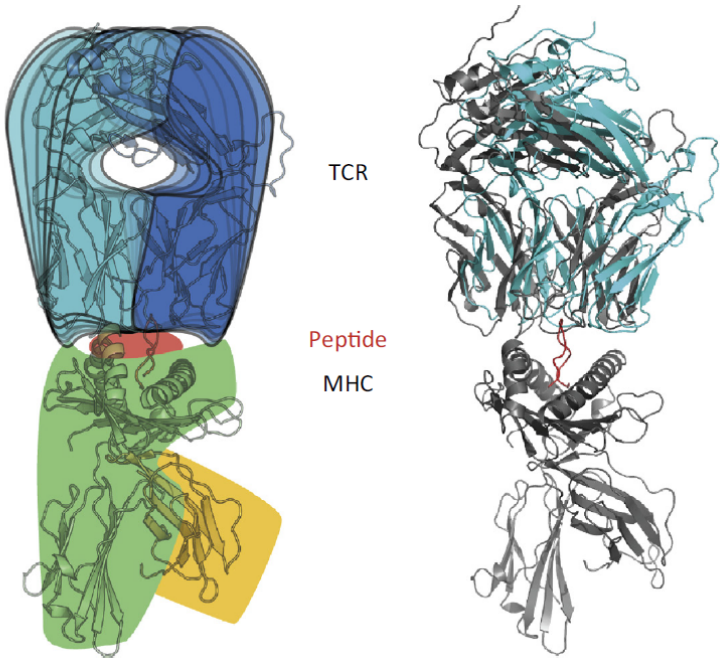

FIGURE 1.2: **Structure of the ligation of peptide major histocompatibility complex (pMHC) class I and T cell receptor (TCR):** The peptide is presented by the MHC complex to the T cell receptor (TCR). The green colored part of the MHC indicates the heavy chain of the pMHC, whereas the light chain (β2m) is colored in yellow. The α and β chains of the TCR are pointed out light and dark blue, respectively. This figure is taken from Kass et al. [28] and modified.

pMHC class I

Peptide major histocompatibility complexes, which fulfill the requirements for class I, are mainly loaded with peptides derived from internally synthesized proteins, which emerge from viral gene products. These proteins are produced from cytosolic proteins by proteolysis within the proteasome and translocated into the rough endoplasmatic reticulum. The produced complex is presented on the cell surface, to which the CD8+ T-lymphocyte can bind [34]. However, binding to an inappropriate TCR does not induce activation of the T-cell [25].

pMHC class II

Via an endocytic process proteins of harmful pathogenic proteins are taken up by an APC. Followed by fragmentation of the endocytosed proteins by proteolytic enzymes in the endosomal/lysosomal compartment, the peptides are expressed and presented on the APC surface embedded in the MHC complex to CD4+ T-lymphocytes. For each individual peptide presented in the MHC complex, a distinct set of T cell receptors are responsible for recognition, which are required due to the high specificity of the individual T cell receptor. The specificity of CD4+ T-lymphocytes allows for recognition of antigens derived from extracellular sources embedded in the MHC class II complex [34].

ICAM-1

To sustain the antigen recognition, adhesion molecules ensure the ligation of the T lymphocyte with the antigen presenting cell [38], [14]. Intercellular adhesion molecule (ICAM) on the APC side and lymphocyte function-associated antigen-1 (LFA-1), which is a member of the integrin family, on the T cell side, interact with each other to establish close contact of the two cells [10].

B7-1

Costimulation factors represent another important group of molecules in the immunological synapse. These molecules, e.g. B7-1, only induce minimal signalling or adhesive characteristics on their own. Instead, they can locally increase adhesion and signalling in combination with other stimuli [14].

1.2.4 T cell receptor - CD3 complex

The complete TCR-CD3 complex, illustrated in figure 1.3, consists of the TCR, which binds to on the surface of antigen presenting cells expressing pMHC, and the CD3 complex, which is responsible for signal transduction [43]. Therefore, the CD3 complex subunits, the cytosolic domains of CD3 γ, δ and ϵ, include copies of the immunoreceptor tyrosine-based activation motifs (ITAMs) [28]. ITAMs are found in a variety of chains associated with immune recognition receptors and appear to be of importance in the signal transduction process by providing a site for interaction of protein tyrosine kinases and the chains to propagate signaling events [6].

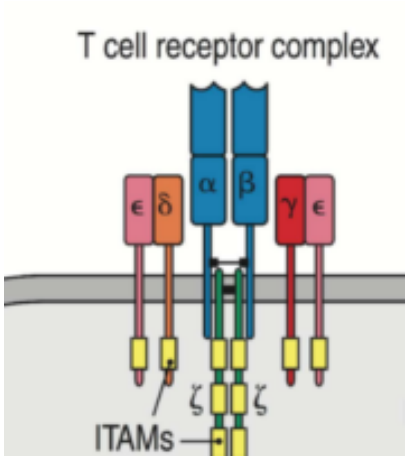

FIGURE 1.3: **Schematic illustration of the structure of the T cell receptor - CD3 complex:** The T cell receptor, which is required for binding to a peptide in a MHC complex presented by an antigen presenting cell, is embedded in a complex with CD3, which is important for signal transduction [34]. The T cell receptor consists of different chains α & β, colored in blue. The cytosolic domains of CD3 complex, γ, δ and ϵ, include copies of the immunoreceptor tyrosine-based activation motifs (ITAMs) [6]. This figure was taken from Murphy [34].

Any process, which induces a biochemical change of the cytoplasmic regions of the CD3 complex upon ligation of TCR:pMHC, is termed 'TCR triggering' [31] [8]. The engagement of TCR:pMHC favours a conformational change of the CD3 complex, which is likely to induce an intracellular signalling cascade [32] [43]. Another important process to trigger signalling of the TCR is the phosphorylation of the ITAMs in the CD3 complex by the Src family tyrosine kinases Lck and Fyn.

Characteristics of the T cell receptor

The T cell receptor, which is illustrated in figure 1.4, is a disulfide-linked heterodimer consisting of different chains (α & β or γ & δ), which belong to the Ig supergene family members and is associated with a set of transmembrane proteins [34].

Important aspects of the TCR antigen recognition include the sensitivity of the TCR, ability to discriminate between self and foreign peptides, versatility and structural diversity [22].

The TCR is able to discriminate between various peptides in the MHC complex, which are expressed on antigen presenting cells (APCs) [22] [24]. Due to the surrounding of the TCR by abundant self-peptides and only a small number of foreign peptides, it is crucial for the TCR to correctly identify harmful peptides. Indeed, the TCR can be triggered by only one single pMHC in the contact area of a T cell and an antigen presenting cell [12] and

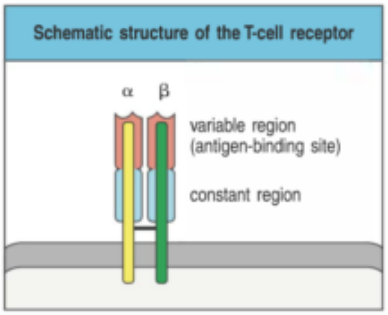

FIGURE 1.4: **Schematic illustration of the structure of the T cell receptor:** The T cell receptor is a disulfide-linked heterodimer, which consists of different chains (α & β, or γ & δ). α, colored in yellow, is a light chain, whereas β, which is highlighted in green, is a heavy chain. Each of these chains has a constant part, shaded in blue, and a variable region, marked in red, which contains the antigen-binding site. This figure was taken from Murphy [34].

is able to discriminate between peptides, which differ by a single amino acid [15].

1.3 Single molecule observations of interaction kinetics of the T cell receptor with pMHC

Different groups used various approaches to characterize the interaction kinetics and to determine interaction duration of the T cell receptor with its ligand, the pMHC (TCR:pMHC). In particular, two groups studied the interaction of live T lymphocytes with an antigen presenting cell mimicking system, supported lipid bilayers containing pMHC and ICAM-1 [19], additionally Huppa et al. [24] anchored B7-1 as well to the artificial cell membrane. While Huppa et al. [24] observed the binding of the T cell receptor to the pMHC with Förster resonance energy transfer (FRET), which is described in the following section, O'Donoghue et al. [19] probed the immobilization of pMHC molecules beneath a T cell with a clever total internal reflection fluorescence microscopy approach, which is also explained in detail in the following section.

Both groups examined the interaction duration of the T cell receptor with the pMHC at different temperatures and varied the density of the pMHC molecules present in the supported lipid bilayer.

By applying single molecule FRET techniques, Huppa et al. [24] observed interaction durations of the TCR:pMHC in the range of seconds at room temperature and approximately 100 ms at physiological temperature (37°C), while the density of pMHC proteins in the bilayer was estimated to be 30

molecules/μm^2. Variation of the density of pMHC molecules at physiological temperatures did not change the interaction duration of the TCR:pMHC. 6 molecules/μm^2 and 150 molecules/μm^2 were investigated and yielded 138 ms and 111 ms, respectively. The exposure time was set to 1 ms.

O'Donoghue et al. [19] determined dwell times of the immobilized trajectories of pMHC proteins beneath the cells. At room temperature dwell times in the range of 5s were observed, as well as at 37°C. These measurements were obtained with a very low density of pMHC molecules, 0.2 molecules/μm^2, in the supported lipid bilayer. By increasing the number of pMHC proteins in the bilayer to 100 molecules/μm^2, the group observed no change in the dwell time of the immobilization duration of the pMHCs. However, this group terms the dwell times of the immobilized trajectories of pMHC "interaction duration" of the T cell receptor with the pMHC and states, that the obtained interaction durations by Huppa et al. [24] are too short. Yet, one of the main differences between the two approaches, is the chosen exposure time. O'Donoghue et al. [19] illuminated their samples for 500 ms. Therefore, they cannot observe any processes shorter than their illumination time. To clarify this discrepancy, this thesis aims to correlate the interaction durations obtained by single molecule FRET measurements with the dwell times of immobilized pMHC molecules in the T cell - supported lipid bilayer interface.

1.4 Fluorescence microscopy

Fluorescence microscopy utilizes fluorophores, which are excited by lasers [33] [46], relaxing upon emission of photons of longer wavelength, which can be detected with sensitive cameras. A high chemical contrast can be achieved via linking a fluorophore to a molecule of interest. Total internal reflection fluorescence microscopy [1] allows for observation of processes in cell membranes adjacent to the glass slide with a high signal-to-noise ratio due to inhibition of background noise of fluorophores which are further away from the site of interest. Förster resonance energy transfer [11], [46] was the method of choice to directly observe the interaction of the TCR and pMHC. These methods allow for observation of interaction of objects in the nm range. Thereby, it is feasible to derive molecular interaction kinetics between the TCR and pMHC.

The resolution in optical microscopy is described by the Rayleigh criterion. Two point sources are regarded as just resolved when the principal diffraction maximum of one image coincides with the first minimum of the other [30]. This distance is given by:

$$R = \frac{0.61 * \lambda}{NA} \tag{1.1}$$

where R is the resolution, λ is the wavelength of the illumination light or the light emitted from the sample, in case of fluorescence microscopy, and NA is the numerical aperture. If one assumes $\lambda = 400\ \mathrm{nm}$ as the shortest visible wavelength, the Rayleigh criterion yields a diffraction limit of approximately 200 nm.

To localize positions of molecules beyond this limit, individual signals need to be further apart than the diffraction limit. Thereby, localizing and tracking of single molecules is possible with single molecule fluorescence microscopy.

1.4.1 Total internal reflection fluorescence (TIRF) microscopy

Total internal reflection fluorescence (TIRF) microscopy allows for selectively exciting fluorophores close to the interface of a cell and a glass slide [1]. Consequently, TIRF microscopy is applied to a broad range of cell biological questions due to the possibility of observing processes at the surface of the membrane of a living cell. With TIRF microscopy one can analyse various parameters of molecules in or close to the cell membrane, which is not obtainable with non-TIRF epifluorescent or confocal microscopy. As in figure 1.5 illustrated, the TIRF excitation field limits the excitation of fluorophores to those close to the cell membrane on the glass slide. The evanescent field has a depth of approximately 100 nm depending on wavelength and angle, hence, fluorophores outside this range are less to negligibly excited, yielding a better signal-to-noise ratio.

The main advantages of TIRF comprise the possibility to access high-contrast images of fluorophores close to the supported lipid bilayer, very low background noise from the bulk of the cell, reduced cellular photodamage, and rapid exposure times [1].

Physical basis of TIRF

The conveniently used configuration of TIRF is through-the-objective TIRF [1], also known as Cis-TIRF, where the laser beam is focused into the back focal plane of the objective lens and shifted in relation to the optical axis. This configuration was also used in this thesis. Upon exiting the objective lens, the laser propagates through the immersion oil into the cover slip, which have matching refractive indices. By entering the aqueous sample, the direction of the laser is altered. If the incident angle of the excitation

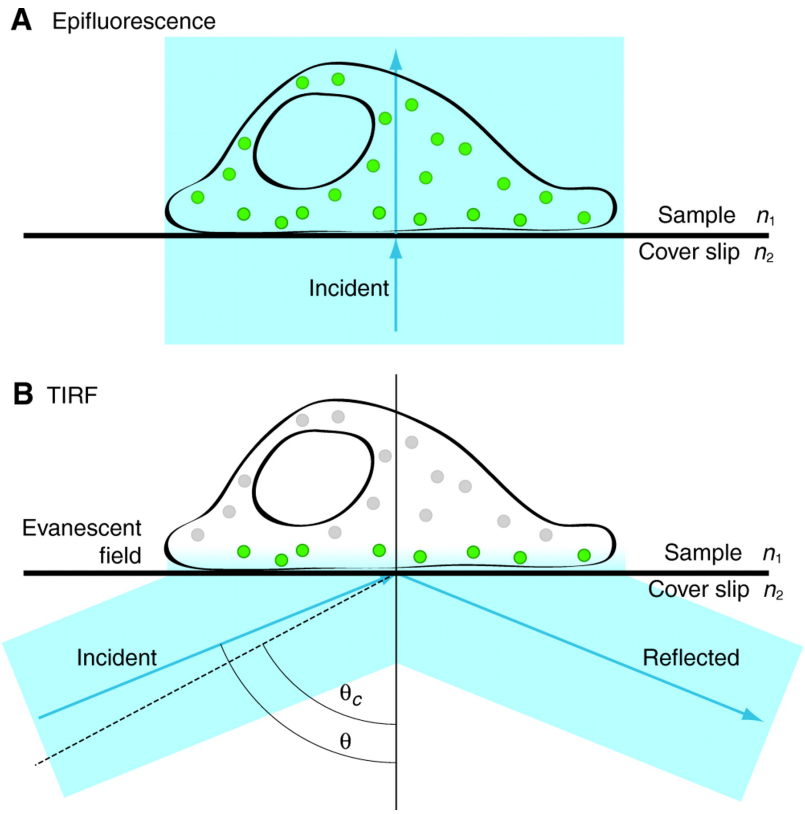

FIGURE 1.5: **Total internal reflection fluorescence (TIRF) microscopy:** illustration of the cover-slip-sample interface. **A:** *Epifluorescent illumination:* the laser beam is perpendicular to the glass slide and, thereby, illuminates all the fluorophores in the sample. **B:** *TIRF:* the laser beam, coming from the left, is coupled to the glass slide under an incident angle, which is greater than the critical angle θ_c. By reflection of the laser beam off the glass slide, an evanescent field is generated on the side of the sample with a penetration depth of approximately 100 nm. The green colored dots indicate, that only fluorophores in close proximity to the glass slide and within the evanescent field are excited. This figure is taken from Mattheyses et al. [1].

beam θ exceeds the 'critical angle', the beam is totally internally reflected and does not enter the sample (figure 1.6). The critical angle is defined by Snell's law in the following:

$$\theta_c = \sin^{-1}(n_1/n_2) \tag{1.2}$$

n_1 and n_2 are the refractive indices of the sample and the glass slide, respectively.

By coupling the laser beam with an incident angle, which is larger than the critical angle θ_c, the laser beam is reflected off the glass slide - sample interface back into the glass slide. Thereby, an evanescent wave, an electromagnetic field, whose penetration depth is limited to the close vicinity of

the glass slide, is created. The evanescent field is responsible for the excitation of the fluorophores at the interface of an, e.g., artificial cell membrane and a T lymphocyte.

The intensity (I) of an evanescent field is exponentially dependent on the distance from the interface (z):

$$I_z = I_0{}^{-z/d} \tag{1.3}$$

I_0 is the intensity of the evanescent field at z=0 and d is the depth of the evanescent field.

This implies, that a fluorophore, which is closer to the interface, is more efficiently excited than a fluorophore further away [1].

The depth of the evanescent field, d, can be calculated with the following equation and gives the distance, at which the excitation intensity is reduced to 1/e of I_0.

$$d = \frac{\lambda_0}{4\pi} \frac{1}{\sqrt{n_2^2 \sin^2\theta - n_1^2}} \tag{1.4}$$

λ_0 is the wavelength of the illuminating laser. Convenient values for the depth of the evanescent field are in the range of 60-100 nm.

The angle of incidence, wavelength, and the refractive indices of the sample and the cover slip influence the depth of the evanescent field [1].

1.4.2 Förster resonance energy transfer (FRET)

The principle of Förster resonance energy transfer (FRET) is the transfer of excitation energy from a donor to an acceptor molecule [11] [46]. The premise for this process are appropriate spectral properties of the donor and acceptor fluorophores. In figure 1.7 the Jablonski energy term schemes are sketched to illustrate the energy transfer from donor to acceptor. By absorption of a photon with a short wavelength, consequently, high energy, the donor gets excited from the ground state S0 to the S1 state, from which it transfers energy to the acceptor. The energy transfer emerges from dipol-dipol interactions of the donor and acceptor molecules and does not require the presence of a photon to transfer the energy.

To induce the energy transfer, the emission spectrum of the donor molecule needs to overlap with the absorption spectrum of the acceptor molecule.

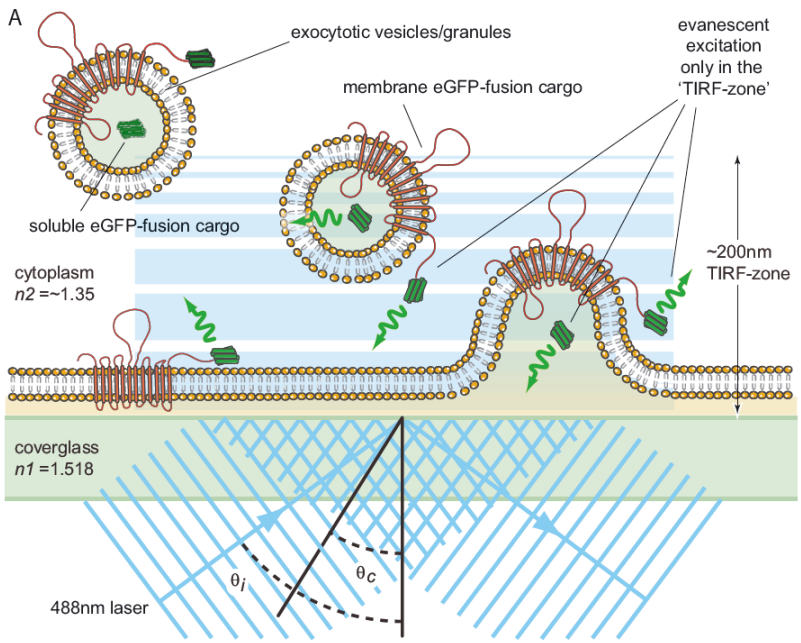

FIGURE 1.6: **Total internal reflection fluorescence (TIRF) microscopy with a supported lipid bilayer on the coverglass:** In objective-based TIRF microscopy the excitation laser is coupled with an incident angle onto the interface between the coverglass and the sample, which is greater than the critical angle θ_c, to generate an evanescent field. Processes in the lipid bilayer can be observed due to the larger depth of the evanescent field compared to the height of the bilayer. Depending on the wavelength, the evanescent field has a depth of approximately 100 nm, whereas the height of the supported lipid bilayer is approximately 8 nm. Thereby, only dyes in the bilayer are excited, but not the dyes further away from the bilayer. This figure was taken from Burchfield et al. [5].

In figure 1.8 the spectra of the used donor and an example for an acceptor fluorophore is shown.

Various parameters influence the efficiency of the Förster resonance energy transfer:

- The extent of spectral overlap of the emission spectrum of the donor fluorophore with the absorption of the acceptor
- The quantum yield of the donor
- The relative orientation of the donor and acceptor transition moments
- The distance between donor and acceptor molecules

The rate of transfer k_T, which is the probability of the transfer of an energy quantum from donor to acceptor per time unit, can be calculated by equation 1.5. This equation is valid for a single donor and acceptor molecule, which are separated by a given distance r.

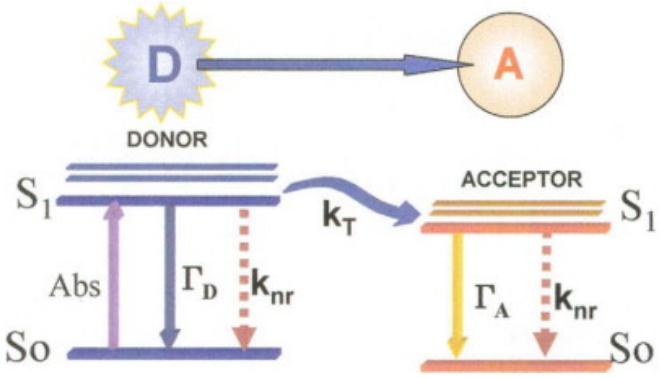

FIGURE 1.7: **Jablonski diagram of the Förster resonance energy transfer process:** Absorption (Abs) of a photon with a short wavelength is required to excite the donor to a state, which allows for the energy transfer to the acceptor molecule (excitation of the donor molecule from S0 to S1 state). k_{T} is the rate of the energy transfer, defined in equation 1.5. The FRET signal is the transition of a photon from the S1 to the S0 state of the acceptor molecule. The relaxation processes from the S1 to the S0 state include the emission rates of the donor and acceptor, Γ_{D} and Γ_{A}, and the rate of nonradiative decay k_{nr}. This figure is taken from Gryczynski [46].

$$k_{\mathrm{T}} = \frac{k^2 Q_{\mathrm{D}}}{r^6 \tau_{\mathrm{D}}} \left(\frac{9000 \cdot \ln(10)}{128(\pi) N_{\mathrm{A}} n^4}\right) J \tag{1.5}$$

Q_{D} is the fluorescence quantum yield of the donor in the absence of the acceptor, τ_{D} gives the lifetime of the donor in the abscence of an acceptor, k^2 is the dipole orientation factor, which describes the relative orientation in space of the transition moment of the donor and acceptor, n is the refractive index of the medium, N_{A} is Avogadro's number, and J is the spectral overlap integral.

The spectral overlap integral J is given as

$$J(\lambda) = \int \overline{f_{\mathrm{D}}}(\lambda) \epsilon_{\mathrm{A}}(\lambda) \lambda^4 d\lambda \tag{1.6}$$

where $\overline{f_{\mathrm{D}}}(\lambda)$ is the donor emission spectrum normalized to unity, and $\epsilon_{\mathrm{A}}(\lambda)$ is the acceptor molar extinction coefficient.

With the following two equations, 1.7 and 1.8, which can be derived from 1.5, the efficiency of the energy transfer 1.10 can be calculated.

$$k_{\mathrm{T}} = \frac{1}{\tau} \left(\frac{R_0}{r}\right)^6 \tag{1.7}$$

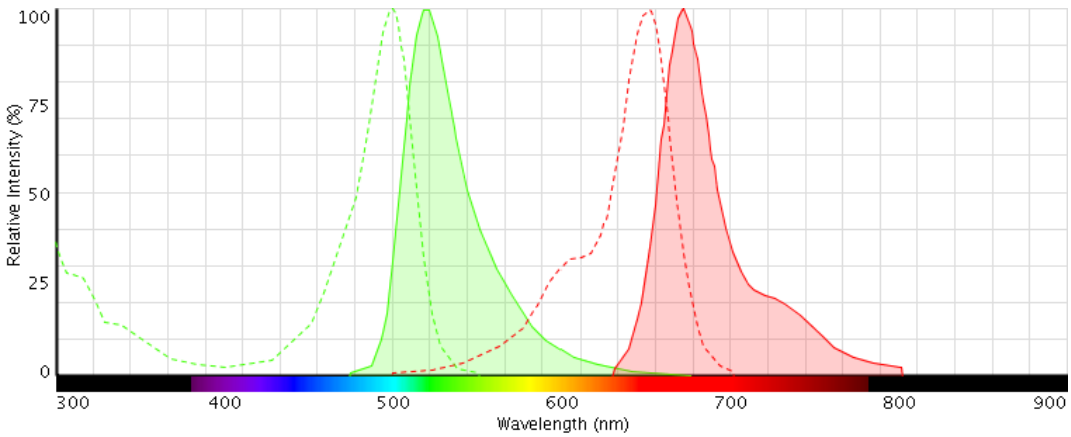

FIGURE 1.8: **Spectra of Alexa Fluor 488 and Alexa Fluor 647:** The dotted lines indicate the absorption spectra, whereas the filled plots show the emission spectra. As required for FRET, the emission spectrum of the donor, Alexa Fluor 488, overlaps with the absorption spectrum of the acceptor, Alexa Fluor 647. In the experiments of this thesis, the fluorophore Atto 655, which has similar spectroscopic properties compared to Alexa Fluor 647, was used. This figure was generated with the *Fluorescence SpectraViewer* on thermofisher.com

$$(R_0)^6 = \frac{9 \cdot \ln(10)}{128(\pi)^5 N_\mathrm{A}} \frac{\kappa^2 Q_\mathrm{D}}{n^4} J \tag{1.8}$$

R_0 is the characteristic Förster distance, the Förster radius, and is usually given in Å.

$$E = \frac{k_\mathrm{T}}{k_\mathrm{T} + \frac{1}{\tau_\mathrm{D}}} \tag{1.9}$$

The efficiency of the energy transfer E depends on the donor-to-acceptor separation distance r with an inverse 6th-power law due to the dipole-dipole coupling mechanism:

$$E = \frac{1}{1 + (\frac{r}{R_0})^6} \tag{1.10}$$

Consequently, the larger the Förster radius, the less critical is the actual distance between donor and acceptor molecule. However, the FRET efficiency is more effective if the donor and the acceptor molecule are in close proximity.

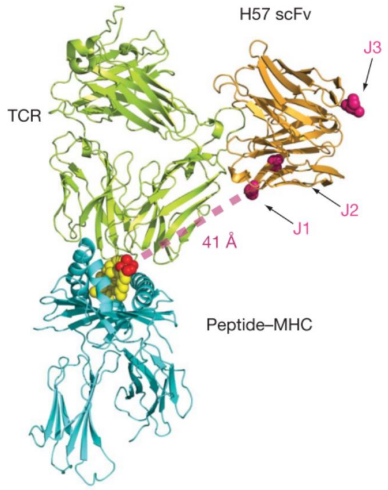

FIGURE 1.9: **TCR - pMHC interaction:** The T cell receptor is labeled with single chain fragment carrying a fluorophore at the proximal position J1. The distance between the fluorophore at the pMHC and the single chain fragment is close enough to provide the necessary proximity for the energy transfer of FRET. This figure is taken from Huppa et al. [24].

FRET between fluorescently labeled pMHC and T cell receptor

For the experiments described in the following, the configuration shown in figure 1.9 was utilized [24]. The peptide histocompatibility complex (pMHC) was labeled as the acceptor and the single chain fragment carrying the donor fluorophore was anchored to the T cell receptor.

To ensure FRET events, the fluorophore was attached to the site of the single chain fragment which is indicated as J1. The distance between the donor and the acceptor molecule was approximately 4.1 nm [24]. This distance is in good agreement with the required radius to obtain FRET events.

1.4.3 Single molecule mircoscopy

In this thesis the interaction of the T cell receptor with pMHC was observed on a single molecule level with TIRF microscopy and single molecule FRET. Inhibition of cellular background noise due to internalized fluorophores or fluorophores, which are further away from the supported lipid membrane - T cell interface, allows via TIRF for resolving single molecule signals embedded in the cell membrane with a higher signal-to-noise ratio (figure 1.10). With single molecule FRET the direct interaction of a single pMHC molecule with a single TCR was observed.

To properly excite and detect single molecules, appropriate fluorophores [37], laser and cameras are required. The quantum yield of the fluorophore

needs to be high enough, furthermore the fluorophore should be as photobleach resistant as possible to provide an photobleaching independent readout. For the appropriate excitation of the fluorophores, excitation power densities in the range of $\mathrm{kW/cm^2}$ are necessary and are provided by lasers. To properly detect the signals, a sensitive camera is needed.

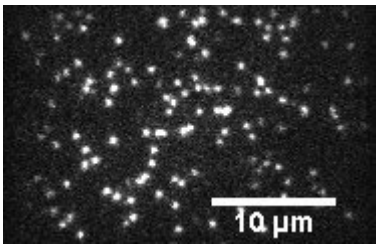

FIGURE 1.10: **Supported lipid bilayer with cholesterol-KK104:** Single molecules are resolved with TIRF microscopy configuration, proper laser powers and a sensitive camera.

Positions of single molecules were determined below the diffraction limit by fitting two-dimensional Gaussian distributions (figure 1.11). Moreover, trajectories could be determined upon connection of the individual positions of single molecule pMHC signals (figure 1.12) [41]. The accuracy of the positions of the individual pMHC molecules was only limited by the localization precision. With the obtained trajectory data various parameters could be evaluated, e.g. diffusion constants and immobilizations of single pMHC molecules.

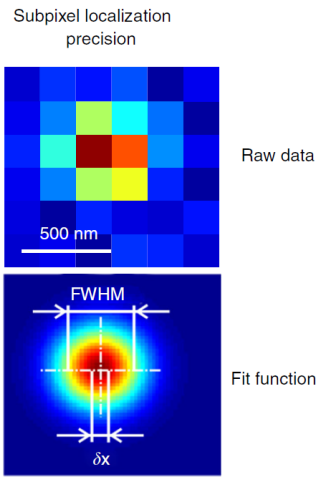

FIGURE 1.11: **Localization precision:** Subpixel localization precision can be achieved by fitting a two-dimensional Gaussian distribution. The classical diffraction limited resolution is determined by the full width half maximum (FWHM), whereas the center of the distribution can be localized to a higher precision. The localization precision is described by δx. This figure was taken from [4].

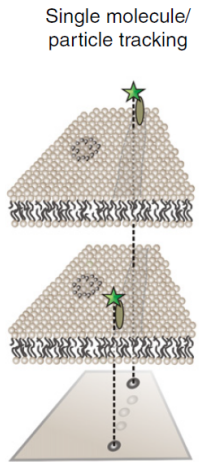

FIGURE 1.12: **A fluorophore, indicated by the green star, attached to a protein diffuses in a supported lipid bilayer:** Trajectories of molecules embedded in an artificial membrane can be determined by connecting individual positions of single molecule signals. Thereby, different characteristics, e.g. diffusion constants or immobilizations, of the molecule of interest can be obtained. This figure was taken from [4].

Advantages of single molecule microscopy

Four main advantages of single molecule microscopy comprise the following aspects [37].

- *Positional accuracy:* To determine the signal distribution of a single molecule signal, Gauss distributions are fitted to the single molecule signals. This approach allows for localization accuracies of single molecule signals below the resolution limit and evaluation of parameters for each single molecule. In [18] Schütz et el. demonstrated postional accuracies of approximately 40 nm. The use of photobleaching resistant dyes allows for longer illumination times and, subsequently, brighter signals. Thereby, the positional accuracy could be improved to approximately 1.5 nm [44].

- *Detailed analysis of heterogenous samples:* individual molecular parameters are accessible to determine the statistical distribution of this parameter. On the contrary, in bulk measurements, only the mean values of the desired parameter of the ensemble can be obtained.

- *Correlation between different parameters:* Due to the possibility of observing various parameters at the same time, it is possible to quantify correlations between these properties. This thesis tries to correlate the immobilizations of trajectories of single molecules with single molecule FRET events.

- *Observation of transitions:* Transitions of different molecular states can be observed directly without the synchronization of the states of the involved molecules as in bulk measurements.

1.5 Single molecule microscopy to decipher pMHC:TCR interactions

In a previous work, the interaction kinetics of pMHC in T cell receptor clusters [3] were obtained in bulk experiments. Under these conditions, fluorescence recovery after photobleaching (FRAP) experiments showed that pMHC molecules anchored to a supported lipid bilayer, mimicking an antigen presenting cell, exchanged within TCR clusters. To determine single molecule interactions between TCR and pMHC, the densities of pMHC in the artificial cell membrane were changed from bulk to single molecule conditions in this thesis. Moreover, these conditions do not only allow for observations between TCR:pMHC, but also for gaining informations about diffusion and immobilizations of pMHC embedded in the supported lipid bilayer.

Analysis of these processes required total internal reflection fluorescence (TIRF) microscopy [1] and single molecule Förster energy transfer (FRET) [20] to derive molecular interaction dynamics at the level of single molecules of the TCR and the pMHC.

It is a field of great interest to understand specific aspects of the interaction of the TCR with the pMHC, for example, the duration of the interaction of pMHC with the TCR. Taken together with diffusion constants and immobilizations of pMHC molecules, a deeper insight in the interaction dynamics of the TCR with the pMHC was gained.

Chapter 2

Materials and Methods

2.1 Sample preparation and cells

2.1.1 5c.c7 T lymphocytes

The group of Huppa (Medical University of Vienna, MUW) prepared and treated the T lymphocytes, which were isolated from murine spleen and blasted with MCC peptide. Two times per week the cells were collected from the Medical University. The T cells were cultured in sterile filtered T Cell Medium (TCM) containing 50ml fetal calf sercum (FCS), 5ml Non-Essential Amino Acids (Lonza, Basel, Switzerland), 5ml Penicillin/ Streptomycin, 10ml L-Glutathione, 500ml RPMI-1640 (Lonza, Basel, Switzerland), 5ml Sodium Pyruvate (Sigma-Aldrich, St. Louis, USA) and 50µM Mercaptoethanol (AppliChem, Gatersleben, Germany).

2.1.2 Lipid bilayer preparation

#1.5 glass slides (Menzel, Jena, Germany) were first wiped with isopropanol or ethanol to remove smears before cleaned in a plasma cleaner to eliminate any organic residues. The glass slides were left for at least 15 minutes in the plasma cleaner. Alternatively, the glass slides were cleaned in Piranha solution, a solution of 35 ml H_2SO_4 (Sigma-Aldrich, St. Louis, USA) and 15 ml H_2O_2 (Sigma-Aldrich, St. Louis, USA), in which the glass slides were incubated for at least 30 minutes. Afterwards, they were rinsed with at least 250 ml deionized H_2O and dried with nitrogen immediately after rinsing.

Nunc Lab-TEK Chambers (Thermo Fisher Scientific, San Diego, USA) were used for all experiments to have multiple bilayers with different properties regarding activation stimuli. While not being used, they were stored in Ethanol (Sigma-Aldrich, St. Louis, USA). To prepare wells for experiments, the plasma or Piranha - cleaned glass slides were glued to the chambers with a two component dental glue.

Preparation of a SLB required a vesicle stock solution containing 90% 1-Palmitoyl-2-oleoylphosphatidylcholine (POPC) and 10% Nickel chelated 1,2-dioleoyl-sn-glycero-3-[(N-(5-amino-1-carboxypentyl)-iminodiacetic acid) - succinyl] (DOGS), which was diluted 1:10 with phosphate buffered saline (PBS, Lonza, Basel, Switzerland). Each well was incubated with 150 µl of this solution for 20 minutes to let the vesicles spread onto the hydrophilic glass slides onto the bottom of the wells.

Subsequently, the wells were rinsed with 25 ml PBS and 330 µl were extracted from each well resulting in a remaining volume of 350 µl per well. The following step included incubation of the wells with additional 50 µl of PBS, containing 0.35 µl and 0.1 µl of His-tagged murine 75 ng/µl ICAM-1 and 50 ng/µl B7-1, respectively, for 75 minutes. For experiments, which required activating lipid bilayers, up to 0.1 µl of the respective pMHC (unlabeled, Alexa Fluor 647, Alexa Fluor 555, Abberiorstar 635, Atto 655) was added. The concentrations of all the pMHC proteins was approximately the same due to the same dilutions yielding the same numbers of molecules in the supported lipid bilayer. Afterwards, the wells were rinsed again with 25 ml PBS two times.

Protein	Amount [µl/Well]	Concentration [ng/µl]	Molecular weight [kDa]	fmol/Well
B7-1	0.1	50	50	0.1
ICAM-1	0.35	75	125	0.21
ICAM-1 488	0.1	240	125	0.192
pMHC 647	0.05	560	50	0.56
pMHC 555	0.05	520	50	0.52

TABLE 2.1: Amount of proteins per Well to achieve approximately 100 molecules/μm^2

For bulk FRET experiments, the number of pMHC molecules in the bilayer was adjusted to be around 100 molecules/μm^2 (table 3.1). To yield a bilayer with properties allowing for localization and tracking of single molecule signals and the possibility to observe single molecule FRET events, the density of acceptor molecules was required to be as low as possible, approximately 0.1-1 pMHC/μm^2. The density of the single chain fragments attached to the T cell receptor yielded an approximate number of 60-70 labeled TCRs/μm^2.

The pMHC proteins, which were anchored via His-tags to the bilayer, included moth cytochrome c (MCC), β2m and T102S. MCC (88–103, ANERADLIAYLKQATK) is a strong agonist, it is the most stimulatory ligand used in these experiments [24]. T102S is a peptide with a modified amino acid sequence (ANERADLIAYLKQA**S**KGGdSdC), having Threonine substituted by Serine at the position 102 of the amino acid sequence, and is,

thereby, supposed to have a weaker binding affinity to the TCR than the MCC peptide. Whereas, β2m is a Null-peptide, an endogenous self peptide [2], and has a completely different amino acid structure (dHdPdPdHdIdEIQMLKNGKKIPGGdSdC). As a negative control, cholesterol with a PEG linker attached KK114 was incubated with the bilayer and experiments were performed and analyzed in the same way as the measurements with the peptides. The cholesterol was a kind gift of Alf Honigmann, Max Plank Institut, Göttingen.

2.1.3 T cell preparation, labelling and sample completion

Approximately one million cells were washed in 1 ml Hank's Balanced Salt Solution (HBSS, Lonza, Basel, Switzerland) and spun down in FACS tubes, afterwards, the supernatant was removed by inverting the tube. Approximately 50 µl of cell suspension remained in the FACS tube.

T cell labelling with single chain fragment

For performing bulk or single molecule FRET experiments, the T lymphocytes were labeled with single chain fragments carrying different fluorphores (Alexa Fluor 555, Alexa Fluor 488, Abberiorstar 635, Alexa Fluor 647). 0.5 – 1 µl of the respective single chain fragment was added, followed by incubation on ice for 20 minutes. Afterwards, the cells were washed three times with cold HBSS to get rid of unbound and to avoid unbinding of bound single chain fragment. All the washing steps were done using a pre-cooled centrifuge (4°C).

To finalize the preparation for the experiments, the buffer in the well was exchanged with imaging buffer by adding and removing 250 µl imaging buffer up to 10 times. 1 to 10 µl of the T cell suspension was injected into the corner of the wells of LabTEK chambers.

Calcium flux preparation

For the acquisition of data from calcium fluxes of T lymphocytes, T cells were loaded with Fura2-AM (Life Technologies, Carlsbad, USA). Approximately one million T lymphocytes were washed and incubated 20 minutes at room temperature on a Thermomixer Comfort at 400 rpm with Fura2-AM, which was diluted 1:200 in 200 µl HBSS + 2% FCS. Afterwards, the cells were washed 3 more times with HBSS and resuspended in 100 µl HBSS. To

perform experiments with these cells, 10 µl were seeded during the recording of a measurement to one well of a LabTEK chamber containing a bilayer with activating or non-activating conditions.

2.2 Lasers, microscopes and camera

For the different experiments, two microscopy set ups were mainly used: tracking experiments, bulk and single molecule FRET measurements were performed on SDT-1 and calcium flux data was acquired on SDT-3.

2.2.1 SDT-1

To properly excite the different fluorophores 3 different lasers were used. The fluorophores, which are excited at 488 nm, e.g. Alexa Fluor 488, required a 488 nm diode laser (Sapphire, Coherent, Santa Clara, USA), whereas, fluorophores like Alexa Fluor 555 were excited with a laser at 532 nm (Millennia X, Spectra Physics, Santa Clara, USA) and a Krypton ion laser at 647 nm (Innova 300, Coherent, Santa Clara, USA) was necessary for the fluorophores Atto 655, Alexa Fluor 647 or Abberiorstar 635. The lasers were controlled by accusto-optical modulators (AOMs; Isomet, Springfield, USA) and subsequently coupled into an inverted light microscope - a Zeiss Axiovert 200 (Zeiss, Jena, Germany) - via multiple mirrors.

To be able to perform experiments with objective-based total internal reflection fluorescence microscopy (TIRFM), a 100x oil-immersion α-plan Apochromat (Zeiss, Jena, Germany) objective with a numerical aperture of 1.46 was used for all measurements on SDT1. A high speed stage (Physik Instrumente (P.I.), Karlsruhe, Germany) was implemtented to shift the laser beam in the back-focal plane providing the desired angle for TIRF. Ever since the objective was accounted for detection and excitation, a quad band TIRF filter (ZT405/488/532/640rpc, Chroma, Bellows Falls, USA) was required to properly remove the laser light from the actual signal.

The DV2 Multichannel Imaging System (Tucson, USA) was placed in front of the camera to be able to collect data, which contains signals from two different excited fluorophores (two color measurements). The required filters (HQ585/40 nm (Chroma) for green or 525/45 nm (Brightline, Semrock) for blue and HQ700/75 nm for red (Chroma)) were used to clean the separated images from the emission and remaining laser light. The signals were detected by an Andor iXon Ultra EMCCD camera (Belfast, UK) cooled down to -60°C for reduction of thermal noise. The laser shutter, the AOM, the

EM-CCD camera and the TIRF illumination were operated by an in-house programmed LabVIEW program (National Instruments, Austin, USA).

2.2.2 SDT-3

T lymphocytes, which were loaded with Fura2-AM, were excited with a monochromatic light source, a Polychrome V (TILL Photonics- FEI Munich, Grafelfing, Germany) at 340 nm and 380 nm. The emitted light was coupled into a Zeiss Axiovert 200M microscope through a Polytrope/Yanus combination by TILL Photonics. For acquisition of images, which contain a large number of cells to be able to statistically analyse calcium fluxes, a UPlanFN 10x air objective (Olympus, Tokyo, Japan) was used. The movies were recorded by an Andor iXon EMCCD camera (Belfast, UK). Live Acquisition 5 (TILL Photonics - FEI Munich, Grafelfing, Germany) was the program to collect images and control the light source.

2.3 Image recording

For the acquisition of movies of the observations, different sequences were programmed to automatize the recording. The timing protocols were either designed directly in the LabVIEW program or with the *SequenceMaker* by Alexander Reismann in MatLab. The Calcium flux experiments were controlled with *LiveAcquisition*.

2.3.1 bulk FRET - Donor recovery after acceptor photobleaching

For the determination of the FRET efficiency of a FRET pair, a protocol, which allows for comparison of the brightness before and after a photobleach pulse, was required (figure 2.1). The illumination protocol included an acquisition of images of the donor and acceptor before and after a photobleach pulse of 500 ms. The illumination time of these images was 5 ms.

2.3.2 Single molecule measurements

For the acquisition of data for diffusion analysis, immobilizations and single molecule FRET events, a protocol was designed to take alternating images of the red and the blue/green channel with an illumination time of 5 ms (figure 2.2). The time delay between a set of red and blue/green images was 10 ms, resulting in a total time lag of 30 ms. The final protocol repeated this sequence up to 200 times to record long enough to detect immobilized

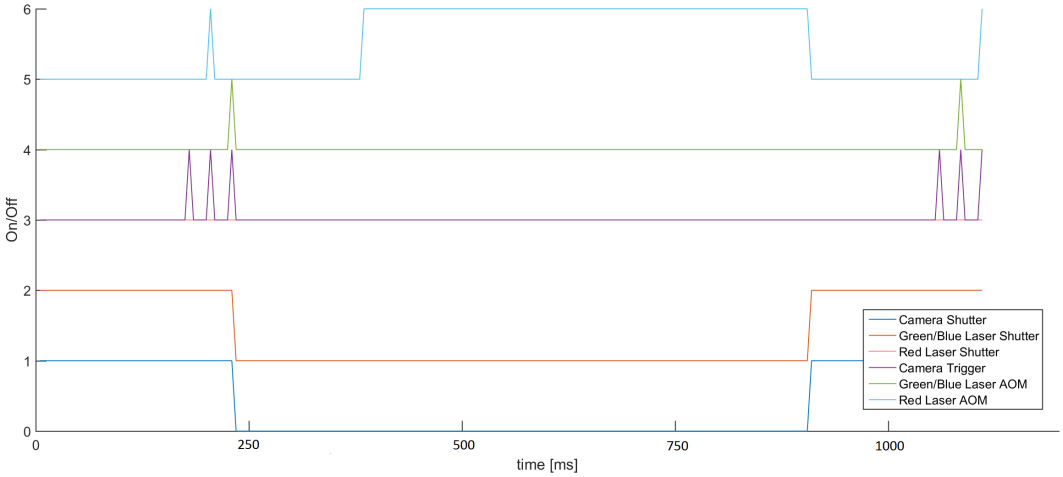

FIGURE 2.1: **Illumination protocol for bulk FRET analysis:** Before and after the photobleaching pulse of 500 ms pictures of the cell and the bilayer with pMHC were recorded with an illumination time of 5 ms to compare the brightness of the respective images. After each application of this protocol a new cell was measured due to bleaching of the acceptor molecules. The red laser shutter was opened the entire timing protocol, therefore, the line indicating the red laser shutter is covered by the line indicating the camera trigger.

molecules and single molecule FRET events. The short delay between the sequences ensured tracking of the particles and, thereby, determining diffusion constants and possible immobilizations. Furthermore, this protocol was used to observe and quantify single molecule FRET events.

2.3.3 Calcium flux measurements

To quantify the calcium flux of T lymphocytes with Fura2-AM it is necessary to obtain alternating images with excitation wavelengths of 340 nm and 380 nm, illumination times of 50 ms and 10 ms and delay times of 54 ms and 45 ms, respectively. Thereby, the total cycle time was 159 ms. The delay between individual image duplets was set to 841 ms. Since it takes the cells some time to respond to a given stimulus, the cells were added to the well after starting the image acquisition. One experiment was recorded up to 15 minutes, which equals a repetition of the sequence of 900 times.

2.4 Image analysis

To determine different aspects of the interaction between the T cell receptor and pMHC, diffusion constants, dwell times of immobilizations and

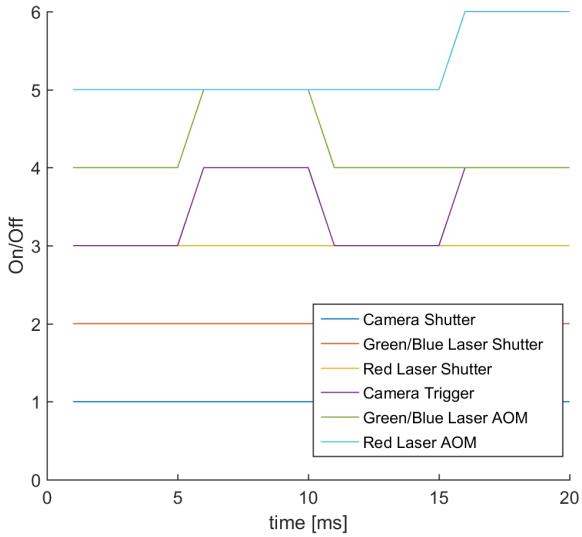

FIGURE 2.2: **Illumination protocol for diffusion constant analysis, immobilizations and single molecule FRET analysis:** 5 ms illumination time with green/blue or red excitation alternated with 5 ms delay, which results in a total of 20 ms duration of one sequence. This illumination sequence was repeated 200 times to obtain enough data to track pMHC molecules and observe sinlge molecule FRET.

localization of single molecule FRET events, were analyzed with different programs.

2.4.1 Single molecule tracking and determination of diffusion constants

particle_tracking_2D, written by Alexander Reismann, localizes and tracks molecules (figure 2.3). For localization, single molecule signals were fitted with Gaussian distributions. *particle_tracking_2D* can connect fitted single molecule signals and, thereby, create trajectories of the molecules. The most important parameters for localizing the single molecule signals are the radius of the found signal, in which the Gaussian distribution is fitted, and the integrated brightness within this radius. In case of tracking one has to set parameters for the allowed maximum distance between two signals in subsequent images, the allowed gap size, which defines how many consecutive frames are allowed to not yield a signal but still be connected by the program, and the minimum track length. For evaluation of the experiments in this thesis, the maximum displacement was usually set to 5 pixels, the allowed gap size was 1 frame and the minimum tracklength was set to be 2 steps. This program provided the necessary data to perform further analysis with *im_moby*.

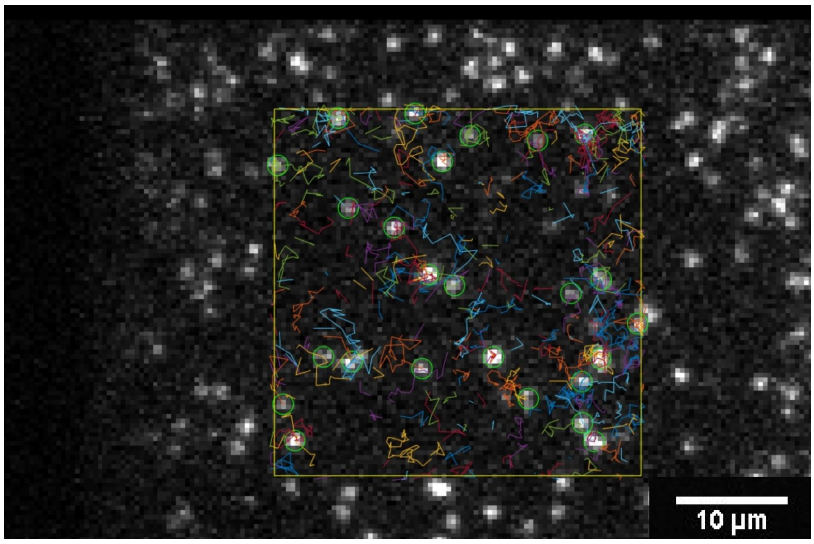

FIGURE 2.3: **Supported lipid bilayer with a low density of localized and tracked pMHC-MCC labeled with Atto 655 fluorophores:** A region of interest (ROI) was chosen to exclude too dense packed molecules from the evaluation of loaclization and tracking. The green circles indicate detected pMHC signals and the vectors in various colors illustrate the corresponding trajectories. The illumination time was 5 ms and the time lag between two images was 30 ms.

Im_moby is a Matlab program written in co-laboration with Martin Fölser, which is able to create a mask out of images of cells, as shown in figure 2.5. This mask is applied to the matrix of the trajectories to discriminate between tracks in and outside of a cell.

msdplot, by Mario Brameshuber, was this final program to calculate diffusion constants. From data, which contained the trajectories of the single molecule signals, the diffusion constants were calculated. Either data from *particle_tracking_2D* or data with sorted trajectories from *Im_moby* can be evaluated by *msdplot*.

As a control, whether single molecule signals have been correctly connected by the *particle_tracking_2D*, *diff_int_correlation_plot* by Mario Brameshuber displayed the single step distribution (figure 2.4). If the histogram has a pronounced "cut", the trajectories have not been correctly associated and a larger maximum distance between the single molecule signals need to be set in the *particle_tracking_2D*.

2.4.2 Analysis of immobilizations beneath and adjacent to a T cell

Single molecule function, *sm_fun*, a program, written by Lukas Schrangl, was used to detect immobilizations and, furthermore, calculate the dwell times. Data, which was fitted with *particle_tracking_2D* to localize and track

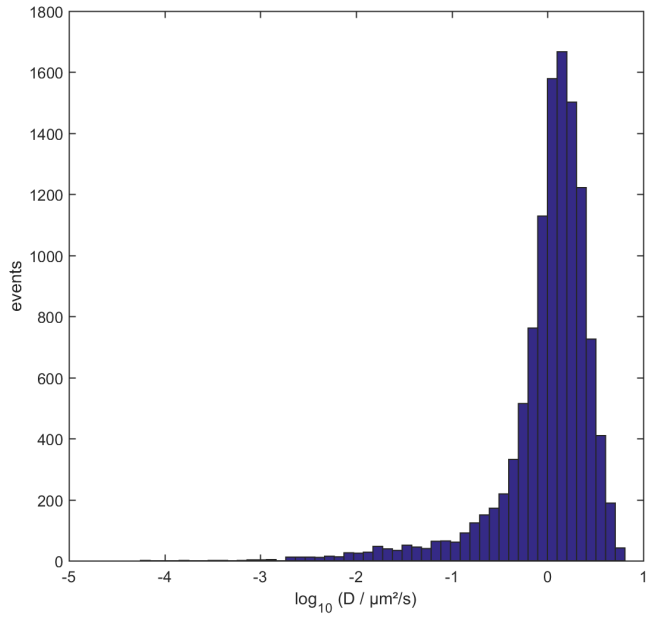

FIGURE 2.4: **Step size distribution of cholesterol validated with *diff_int_correlation_plot* by Mario Brameshuber:** After the generation of trajectories with *particle_tracking_2D*, a program to control the distribution of the step sizes was applied.

the single molecule signals and sorted by *Im_moby* to disentangle trajcetories beneath and adjacent to the T cell, was further analyzed with *sm_fun*. Two different algorithms were implemented to determine immobilizations, which are described in the following.

Close vicinity

The algorithm considers a radius, which is chosen depending on the diffusion constant of the respective particle, around single molecule signals to only connect particles, which remain in close vicinity: each position of a particle has to remain in the mean of the radii of consecutive and previous steps. This ensures that the particle does not slowly drift and only particles which are really immobilized are recognized as immobilizations. Based on the number of frames, in which the immobilization occurs, the dwell time can be estimated. The multiplication of the number of consecutively detected immobilizations with the time lag yields the duration of the immobilization.

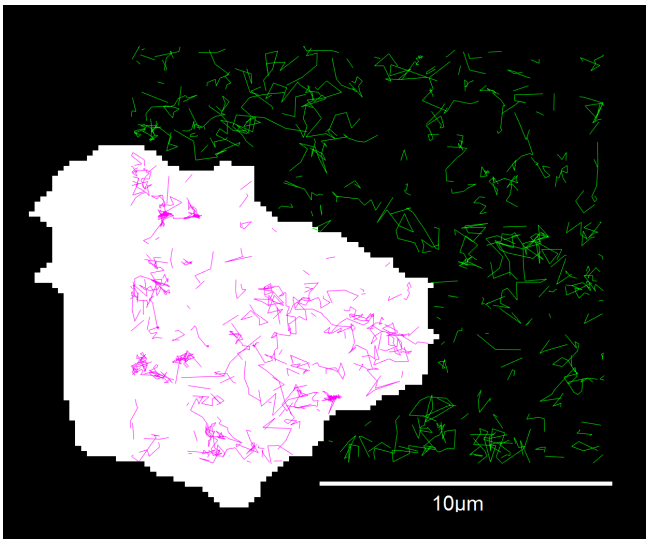

FIGURE 2.5: **Mask of the cell to distinguish between the trajectories beneath and adjacent to the T cell:** After the generation of trajectories with *particle_tracking_2D*, a program to localize and track single molecule signals, *Im_moby*, which creates a mask and, thereby, separates between beneath and adjacent to the T cell, was applied. The magenta or green trajectories illustrate if a trajectory is beneath or adjacent to the T cell.

Center of mass

This approach calculates the center of mass of subtrajectories of single molecule trajectories in a given radius and chosen minimum step length. An immobilization is only detected, if enough steps are found within a certain radius over a certain time. Comparably to the close vicinity approach, the radius and the minimum duration are arbitrarily chosen. In this algorithm tolerances are implemented: these tolerances determine, how many steps are allowed to exceed the chosen radius. The relative tolerance determines the percentage of the steps within the chosen radius, which are allowed to be outside the radius. Whereas, the absoulte tolerance is set to an absolut number of steps, which are allowed to exceed the radius. The algorithm always uses the smaller number of steps, which exceed the radius, to determine an immobilization. In the evaluation of the following experiments, the relative tolerance was set to 5%, the radius was chosen to be 1 pixel and the minimum duration was set to 5 frames.

2.4.3 Bulk FRET analysis

For the evaluation of the donor recovery after acceptor photobleaching (DRAAP) measurements *ImageJ* was the first approach to quantify the brightness of

the donor molecules before and after the photobleaching. A region of interest (ROI) in the middle of the T cell, around the cSMAC, as shown in figure 3.7, was chosen to determine the ratio of the brightness before and after the bleaching process. To compensate for bleaching of the donor for recording the two images, a negative control, where the bleaching laser was blocked, served as a reference to normalize the data. For every bulk FRET analysis, the bulk FRET efficiency was averaged over at least 30 T cells. *Excel* was used to determine the average bulk FRET efficiency.

2.4.4 Single molecule FRET analysis

For the evaluation of single molecule FRET events, *Coloc*, a program written in python by Lukas Schrangl was applied. This algorithm is capable of detecting localizations, tracking particles and colocalizing directly excited donor signal of pMHC signals with single molecule FRET events. The localization and tracking algorithms are the same as in Alexander Reismann's "particle_tracking_2D". Additionally, a colocalization algorithm was implemented to correlate single pMHC signals with single molecule FRET events. Correlation of the directly excited donor signal of pMHC signals with single molecule FRET events ensured, that the detected single molecule FRET signals were indeed smFRET events and not artifacts, ever since single molecule FRET events are very dim and sometimes hard to interpret, as demonstrated in figure 3.8. The duration of the single molecule FRET events was estimated in the same way as the immobilizations: the number of connected frames showing a single molecule FRET event was multiplied with the time lag.

2.4.5 Colocalization of single molecule FRET events and immobilizations

Correlation of immobilizations with single molecule FRET events was evaluated with Lukas Schrangls' *FRET-Immob Coloc*. The lastest version, which was used for evaluation of the data presented in this thesis, is 4.0.

With *FRET-Immob Coloc* it is feasible to localize and track pMHC signals, determining immobilizations and correlating found immobilizations with single molecule FRET events. The implemented algorithms are explained in the previous sections.

2.4.6 Calcium flux analysis

The main program for quantitative analysis, checking the quality of the images/movies or visual analysis of Calcium fluxes, was ImageJ. An in-house plug-in for ImageJ allows for visual quantification of calcium flux. The Calcium flux can be identified by analyzing subsequent images.

Qualitative analysis was performed with Matlab. *mCalcium*, written by Martin Fölser, localizes and tracks cells, uses the trajectories to analyse the brightness and calculates the ratio between the 340/380 nm images of the calcium flux experiments.

Chapter 3

Experiments and Results

3.1 Characterization of the functionalized supported lipid bilayer

Control experiments for determination of the appropriate conditions were performed before characteristics of the T cell receptor - peptide major histocompatibility complex (TCR:pMHC) interaction were measured. Thus, a density analysis of the proteins anchored to the lipid bilayer - purchased ICAM-1, various pMHCs and B7-1 - preceded the main experiments of this thesis. If not otherwise indicated, the pMHC carried the stimulatory moth cytochrome C (MCC) peptide in its major grove.

Figure 3.1 shows the interaction of a T cell with an antigen presenting cell (APC) mimicking system. pMHC, ICAM-1 and B7-1 are anchored via His_6-tags to a supported lipid bilayer, providing an environment to the T cell for adhesion and interaction with the proteins. On the side of the T cell, the co-receptors/ligands of pMHC, ICAM-1 and B7-1 are illustrated: the T cell receptor, responsible for activation of the T cell upon binding to pMHC, LFA-1, attaching the cell to the bilayer by binding to ICAM-1, and CTLA-4, binding to B7-1 and providing co-stimulatory signals [6].

To test for proper activation of the T lymphocytes, T cells were seeded onto bilayers containing different densities of pMHC complexes and, subsequently, Calcium flux was measured. Thereby, "activating" and "non-activating" conditions were determined for diffusion analysis and immobilization/single molecule FRET measurements.

3.1.1 Density of commercial ICAM-1

One control included testing of the purchased ICAM-1. The main difference between the commercial ICAM-1 and the ICAM-1 produced by the *Medizinische Universität Wien (MUW)* is the number of His-tags. The commercial ICAM-1 is anchored to the bilayer via 6 instead of 12 His-tags [36].

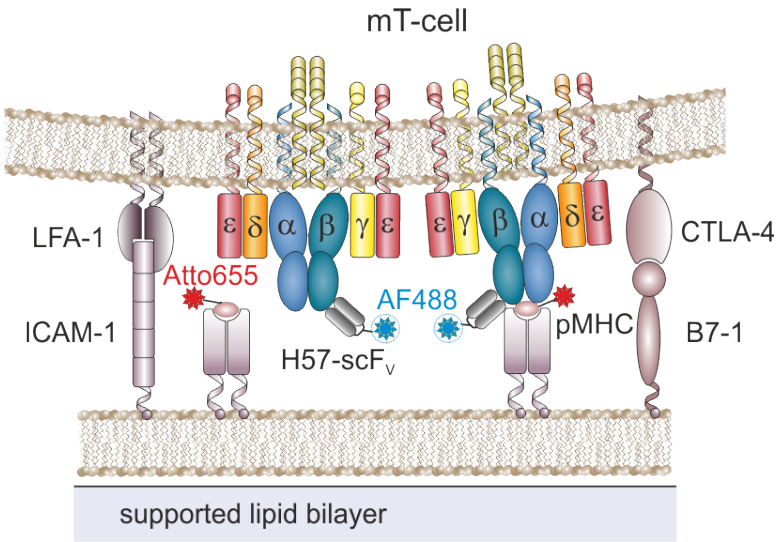

FIGURE 3.1: **Schematic illustration of a supported lipid bilayer with anchored proteins and T lymphocyte with attached single chain fragment:** For single molecule FRET observations between T cell receptor and pMHC, pMHC labeled with Atto 655, unlabeled ICAM-1 and B7-1 were anchored to a supported lipid bilayer to provide adhesion stimuli and co-stimulatory conditions to the T cell. The T cell receptor was labeled with a single chain fragment (scFv) carrying an Alexa Fluor 488 fluorophore. This configuration of pMHC-Atto-655 and scFv-Alexa Fluor-488 allowed for detection of single molecule FRET events, discussed in following parts of this thesis. This figure was kindly provided by Mario Brameshuber.

Hence, a measurement to test the lifetime of the anchoring of the ICAM-1 to the bilayer was performed. Due to the fewer His-tags the commercial ICAM-1 was suspected to be less stably anchored to the supported lipid bilayer compared to the the ICAM-1 with 12 His-tags. A bilayer (figure 3.1) with fluorescently labeled ICAM-1 was prepared following the protocol in the *Materials and Methods* section. Alexa Fluor 488 was attached to ICAM-1 via a NHS-ester. In this control experiment, only ICAM-1 was embedded in the supported lipid bilayer and no cells were seeded on the artificial cell membrane, whereas in figure 3.1 all the significant proteins, pMHC, ICAM-1 and B7-1, and the interaction with the T lymphocyte are illustrated. The density of ICAM-1 was adjusted to be 100-200 molecules/μm^2 by testing different dilutions of the stock solution. An amount of 0.21 fmol was finally added to each well, resulting in a density of approximately 200 molecules/μm^2.

For the duration of two hours the brightness of the bilayer on different positions was recorded every 15 minutes to determine the time course of the brightness of ICAM-1 signals (figure 3.2). Under these conditions the measurement showed no decrease in the brightness of ICAM-1 signals as

function of time, leading to the conclusion that ICAM-1 remains sufficiently stable anchored to the supported lipid bilayer.

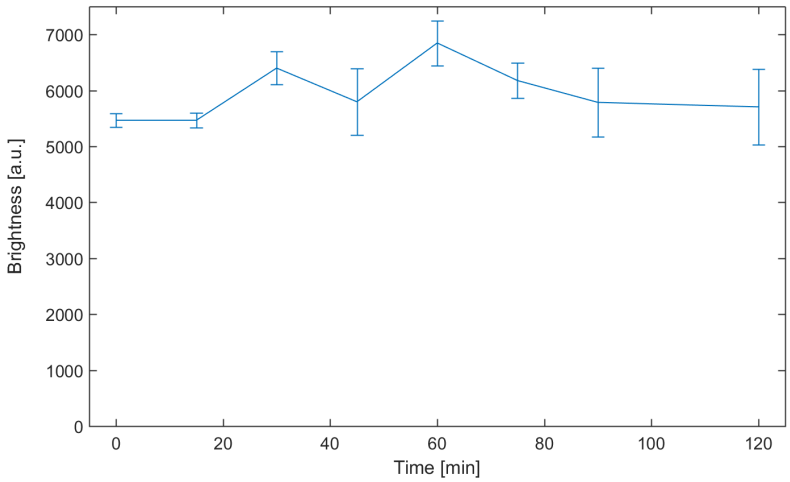

FIGURE 3.2: **Time dependence of ICAM-1 during 2 hours:** By using 0.21 fmol ICAM-1 labeled with Alexa Fluor 488 dye a bilayer with a surface density of approximately 200 molecules/μm^2 was prepared. The brightness of different positions of a bilayer was measured every 15 minutes to control the anchoring of the ICAM-1 to the lipid bilayer. No reduction of the brightness of the ICAM-1 signals was observed, allowing for the conclusion that ICAM-1 remains stably anchored to the supported lipid bilayer.

3.1.2 Density of pMHC, ICAM-1 and B7-1

A decisive parameter to control the responses of T cells is the number of molecules anchored to the supported lipid bilayer. Upon the exposure of the T cell to high densities of pMHC, the activation of T cells is induced. ICAM-1 is required for the adhesion of the T cells to the bilayer and B7-1 is a co-stimulatory factor, effecting Calcium flux experiments by elongating the Calcium flux signal of the T cell [35]. Consequently, further control measurements were performed to test the required amount of pMHC, ICAM-1 and B7-1 to obtain the stimulatory conditions of interest.

The brightness of single fluorophores was determined in a separate experiment by incubating the bilayer with only trace amounts of the respective labeled proteins, pMHC Abberiorstar 635, pMHC Alexa Fluor 647, pMHC Atto 655 or ICAM-1 Alexa Fluor 488. With this information, the density of the bulk was estimated by dividing the bulk brightness by the brightness of a single molecule.

The required amount of B7-1 was estimated based on the molecular weight, concentration of the stock solution and by comparison with the characterized ICAM-1. By assuming a proportional relationship between the amount

Protein	Amount [µl/well]	Concentration [ng/µl]	Molecular weight [kDa]	fmol/well
B7-1	0.1	50	50	0.1
ICAM-1	0.35	75	125	0.21
ICAM-1 488	0.1	240	125	0.192
pMHC 647	0.05	560	50	0.56
pMHC 555	0.05	520	50	0.52

TABLE 3.1: Amount of proteins per well to obtain approximately 100 molecules/μm^2

of protein per well, A, concentration, C, and molecular weight, MW, the required amount of B7-1 was estimated by

$$A_{\text{B7-1}} = \frac{A_{\text{ICAM-1}} \cdot C_{\text{ICAM-1}} \cdot MW_{\text{B7-1}}}{MW_{\text{ICAM-1}} \cdot C_{\text{B7-1}}} \tag{3.1}$$

The same densities of ICAM-1 and B7-1 were used in all experiments to allow for comparable conditions. The number of molecules was approximately 100-200 molecules/μm^2 to exhibit proper adhesion and co-stimulatory conditions [36].

The number of pMHC complexes in the bilayer depended on the particular experiment. In table 3.1 the amounts of proteins to achieve densities of approximately 100 molecules/μm^2, necessary for activating conditions of the lipid bilayer, are shown. On the contrary, the number of pMHC in the bilayer for non-activating conditions was 0.1-1 molecule/μm^2. Although there is evidence in the literatur, that one pMHC molecule is sufficient to induce the activation of a T cell in case of cell-cell interactions [16], no microcluster, c-SMAC formation or Calcium flux was observed under these conditions, as shown in the *Characterization of activating/non-activating conditions* section.

In table 3.1 the amounts of proteins required to achieve densities of .... necessary fir activating cond. of the lipid bilayer are shown

3.1.3 Imaging buffer considerations

The diffusion constants of pMHCs anchored to the lipid bilayer were used as an indication for the interaction between the T cell receptor with its ligand, the pMHC. Upon exchange of buffer - a standard routine for performing T cell experiments - a large spread in diffusion constants over time of pMHC MCC, T102S, β2m and cholesterol was observed. The fetal calf serum (FCS) contained in the imaging buffer was suspected to influence the quality of the bilayer. Thus, an imaging buffer used in Axmann et al. [2]

- HBSS containing 1% ovalbumin - was tested. Whether this imaging buffer has less influence on the properties of the bilayer than the HBSS + 2% FCS has not been characterized yet.

For verification of quality changes of the bilayer, the influence of different imaging buffer, PBS, pure HBSS, HBSS + 2% FCS and HBSS + 1% ovalbumine, was tested. Supported lipid bilayer with pMHC Abberiorstar 635, ICAM-1 and B7-1 were prepared following the protocol described in the *Materials and Methods* section. Trace amounts (0.1-1 molecule/μm^2) of fluorescently labeled pMHC were required to unambiguously localize and track freely diffusing molecules to determine the diffusion constant.

First, the diffusion constant of pMHC Abberiorstar 635 anchored to the lipid bilayers was measured without a buffer exchange. The solution in the well only contained phosphate buffered saline (PBS). A total of 5 measurements were recorded every 15 minutes. These controls showed diffusion constants of approximately 1.1 $\mu m^2/s$. As expected, the diffusion constant did not change for the entire measurement time of 60 minutes (figure 3.3, blue line) showing that PBS did not impair the quality of the lipid bilayer.

Furthermore, to exclude an influence of the Hank's balanced salt solution (HBSS) alone on the quality of the supported lipid bilayer, the buffer was exchanged to pure HBSS. To compare the previous experiment with this measurement, a total of 5 measurements every 15 minutes was recorded as well. The diffusion constant of the fluorescently labeled pMHC under this condition was determined to be 0.9 $\mu m^2/s$, thereby, a decrease by 13.6% compared to the diffusion constant of pMHC in pure PBS was observed. During the duration of the experiment the diffusion constant did not show any further reduction (3.3, orange line).

After the exchange of PBS to Hank's balanced salt solution (HBSS), now including 2% FCS, the diffusion constant of pMHC was instantly reduced by 42.1% to 0.63 $\mu m^2/s$ compared to the diffusion constant of pMHC in pure PBS (3.3, yellow line). After 15 minutes the diffusion constant decreased further by more than 44.5% compared to the initial diffusion constant of pMHC in the imaging buffer solution, HBSS + 2% FCS. 30 minutes after the buffer exchange the diffusion constant showed a reduction to 0.22 $\mu m^2/s$ which is a decrease by 65.1% compared to the first measured diffusion constant of pMHC in this imaging buffer. A later measurement at a time point of 60 minutes showed a further decrease. This control revealed the issues with the FCS containing imaging buffer.

For the imaging buffer containing 1% ovalbumin, the first measured diffusion constant of pMHC was 0.68 $\mu m^2/s$, showing a decrease of 37.83% compared to the initial diffusion constant in PBS (3.3, purple line). This first

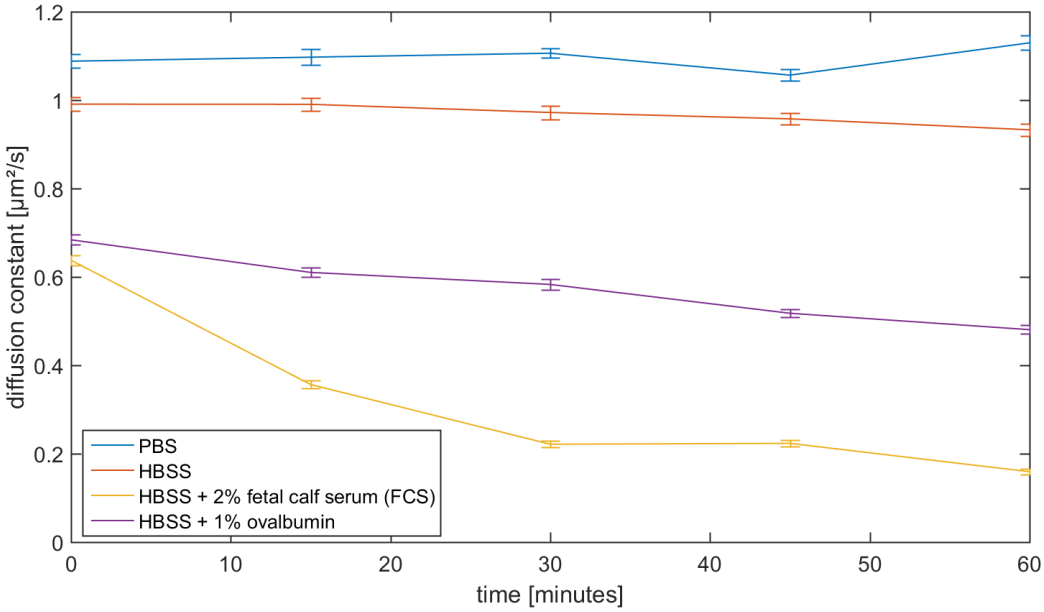

FIGURE 3.3: **Comparison of the time dependence of the diffusion constants of pMHC in a supported lipid bilayer with different imaging buffers:** PBS, HBSS, HBSS + 1% ovalbumine, HBSS + 2% FCS. Upon changing of the buffer from PBS to an imaging buffer, the diffusion constant decreased significantly - the most significant decrease of the diffusion constant was observed for a buffer containing 2% FCS.

reduction is comparable to HBSS + 2% FCS, however, the subsequent decline of the diffusion constant in HBSS + 1% ovalbumine was significantly less compared to HBSS + 2% FCS. After 15 and 30 minutes the obtained diffusion constant was comparable to the start value. A further decrease of the diffusion constant was observable after 60 minutes. These data suggest, that it is possible to collect data at least for 60 minutes without a major change in the diffusion constant in the bilayer with a HBSS buffer containing 1% ovalbumine.

3.1.4 Characterization of activating/non-activating conditions

Determination of activation triggering conditions of the supported lipid bilayer was decisive to define "activating" and "non-activating" conditions.

Following the bilayer preparation and Calcium measurement protocol in the *Materials and Methods* section, T cells were loaded with the ratiometric Fura-2AM dye. Upon starting the illumination sequence to obtain alternating images with 340 nm and 380 nm excitation, the T cells were seeded onto supported lipid bilayer containing low densities of pMHC Atto 655 (0.1-1

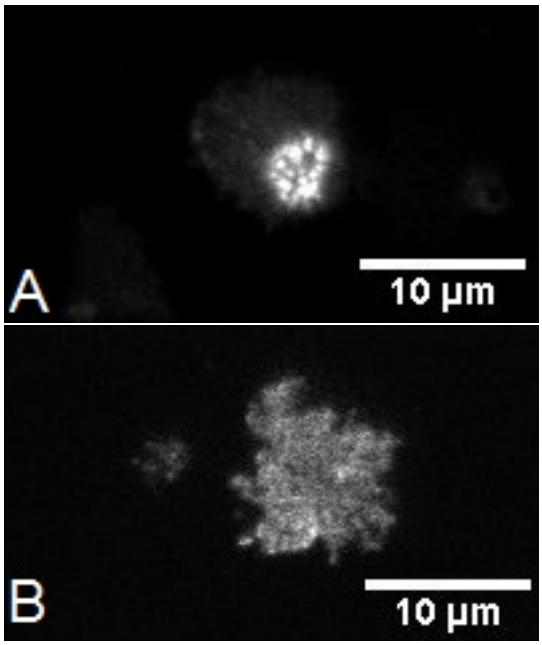

FIGURE 3.4: **Activating and non-activating cell:** T cells were added to lipid bilayers containing ICAM-1, B7-1 and pMHC.
A: The T cell responded to a stimuli of a high density (approximately 100 molecules/μm^2) of pMHC by forming microclusters and dragging them into the cSMAC.
B: No response of the T cell after adhesion to the supported lipid bilayer containing 0.1-1 pMHC molecules/μm^2.
The two figures do not exhibit the same scaling.

molecules/μm^2) or high densities of pMHC Atto 655 (approximately 100 molecules/μm^2) conditions.

Low densities of pMHC Atto 655 (0.1-1 molecules/μm^2) did not induce the activation of cells (figures 3.4 and 3.5, B) and fulfilled the requirements of unambiguous single molecule detection and, hence, determination of diffusion constants and immobilizations, and single molecule FRET measurements. On the contrary, cells seeded onto bilayers containing high densities of approximately 100 pMHC Atto 655 molecules/μm^2 exhibited the expected behavior by showing cSMACs (figure 3.4, A), and Calcium flux (figure 3.5, A).

For subsequent experiments under activating conditions, bilayers containing approximately 100 unlabeled pMHC molecules/μm^2 and 0.1-1 labeled pMHC Atto 655 molecules/μm^2 were prepared. Under these conditions the cells showed similar Calcium flux (figure 3.6) and microcluster/cSMAC formation (data not shown) compared to the high density of pMHC Atto 655. The mixture of unlabeled and labeled pMHC exhibited activating conditions with appropriate properties to localize and track single pMHC Atto 655 molecules allowing for diffusion analysis, detection of immobilizations

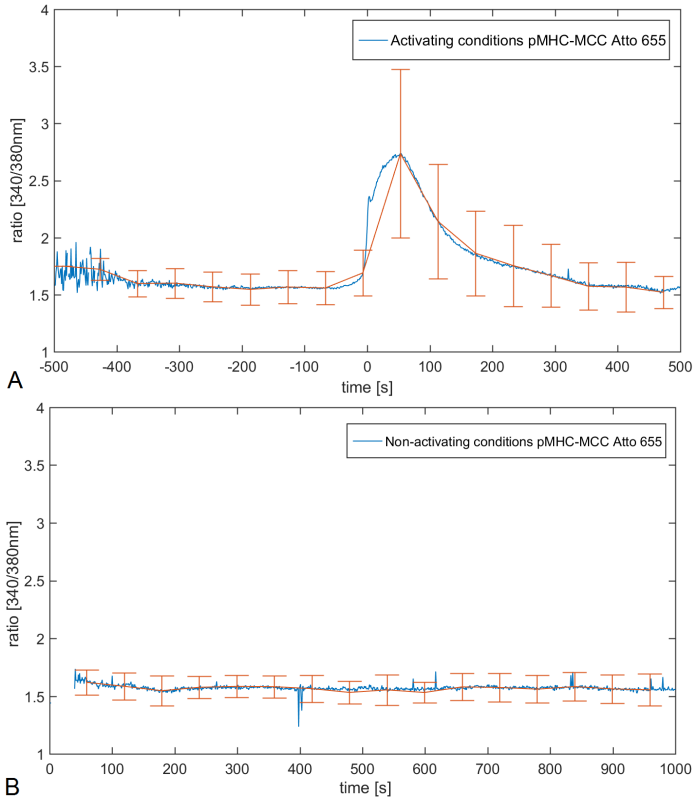

FIGURE 3.5: **Calcium flux upon activating stimuli and non-activating conditions with pMHC Atto 655:** During image acquisition, 5c.c7 T cells were seeded onto the bilayer containing ICAM-1, B7-1 and different densities of pMHC Atto 655. For evaluation of the average-value curve, the mean of the Calcium flux data of approximately 500 T cells was taken.
A: A high density of 100 pMHC Atto 655 molecules/μm^2 triggered the Calcium flux of T cells. Time point = 0 indicates the activation of the T cells.
B: A low density of approximately 0.1-1 pMHC Atto 655 molecules/μm^2 did not induce an activation of the T cells.

and single molecule FRET events.

3.1.5 Selection of the optimum FRET pair (bulk FRET analysis)

Different fluorescently labeled pMHCs and single chain fragments (scFv) were tested to determine the most efficient FRET pair. To measure the efficiency of the FRET pairs, bulk FRET experiments, requiring a high surface density of fluorescently labeled T cell receptor (60-70 scFv/μm^2) and pMHC (100 pMHC molecules/μm^2), the latter anchored to the supported lipid bilayer, were performed. Under these conditions, high bulk FRET signals were obtained. One approach to quantitatively measure bulk FRET efficiencies is "Donor Recovery After Acceptor Photobleaching" (DRAAP). Upon photobleaching of the acceptor, the donor dequenches, yielding a higher

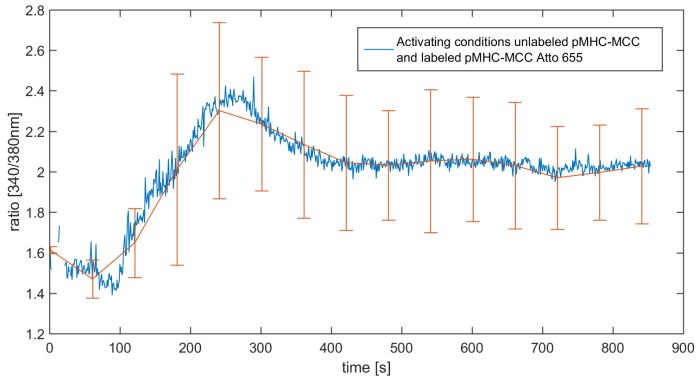

FIGURE 3.6: **Calcium flux upon activating stimuli by unlabeled pMHC and pMHC labeled with Atto 655:** A high density of 100 unlabeled pMHC molecules/μm^2 and 0.1-1 pMHC Atto 655 molecules/μm^2 triggered Calcium flux of T cells upon adhesion and activation on the artificial cell membrane.

donor brightness (figure 3.7). Due to accumulation of TCRs in the cSMAC, the bulk FRET signal yielded the highest values in the red encircled regions (figure 3.7, A and B). By comparing the brightness of the cSMAC before and after the acceptor bleaching, the bulk FRET efficiency can be estimated with

$$E_{\text{bulk}} = 1 - \frac{B_{\text{before}}}{B_{\text{after}}} \tag{3.2}$$

where E_{bulk} is the bulk FRET efficiency, B_{before} is the brightness of the donor before and B_{after} is the brightness of the donor after photobleaching.

Huppa et al. [24] determined in their FRET studies between pMHC and the T cell receptor FRET efficiencies of approximately 10%. However, the fluorophores used in this paper are prone to photobleaching, which is not applicable for the experiments of this thesis, because strong photobleaching would limit single molecule tracking experiments. Consequently, a FRET pair with photobleaching resistant fluorophores was the objective.

Bulk FRET experiments with pMHC labeled with Alexa Fluor 647 or Atto 655 as acceptor and single chain fragment labeled with Alexa Fluor 555 as donor yielded low FRET efficiencies (table 3.2).

	pMHC-647	pMHC-655	pMHC-635
Average E_{bulk} in [%]	2.75	2.24	1.02
Standard deviation	2.45	3.5	2.6

TABLE 3.2: **Bulk FRET analysis with various labeled pMHC and single chain fragment J1-555:** The average bulk efficiency was determined with equation 3.2 and the donor brightness before and after acceptor photobleaching, as explained in the text.

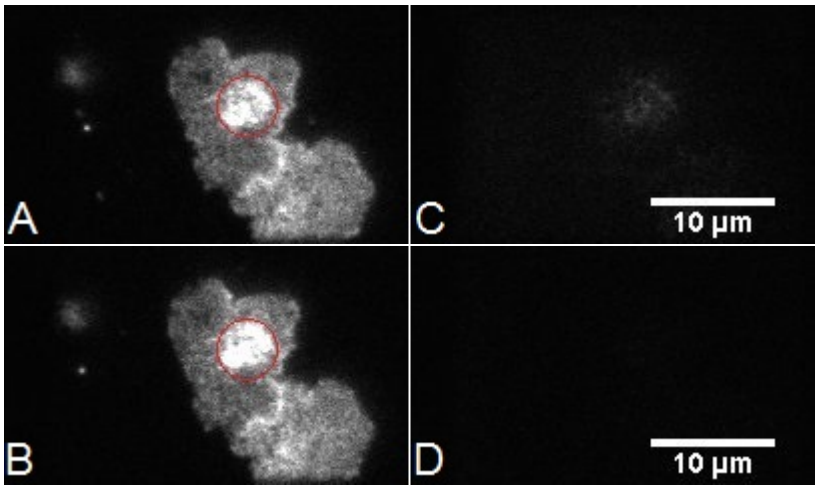

FIGURE 3.7: **Donor recovery after acceptor photobleaching experiment:** T cells were seeded onto a supported lipid bilayer exhibiting an activating environment (100 pMHC molecules/μm^2), indicated by the cSMACs red encircled in (A) and (B). The red circle shows the area used for subsequent brightness analysis of the the donor signal before (A) and after photobleaching of the acceptor (B). A clear increase in donor brightness is observed (B), which correlates well with the disappearance of the FRET signal (compare (C) with (D)).

In order to obtain a potentially higher bulk FRET efficiency, a different donor was tested. The fluorophore Alexa Fluor 555 was substituted by Alexa Fluor 488. The single chain fragment labeled with this fluorophore exhibited several advantages for the subsequent single molecule FRET measurements: a negligible donor bleed through into the acceptor channel and insignificant acceptor cross-excitation. Bleed-through exhibits a problem, if the donor molecule is excited with high laser power required for single molecule FRET. The excitation maxima of the donor, 488 nm, and acceptor, 655 nm, are further apart compared to the previous FRET pairs, 555 nm and 647/655 nm and thereby favorable for circumventing acceptor cross-excitation. The bulk FRET efficiency for this FRET pair yielded on average 7.8% (table 3.3). Hence, this FRET pair was further used for single molecule FRET and tracking measurements.

	pMHC-647	pMHC-655	pMHC-635
Average E_{bulk} in [%]	0.8	7.82	0.9
Standard deviation	3.14	5.12	1.1

TABLE 3.3: **Bulk FRET analysis with various labeled pMHC and single chain fragment J1-488:** For the determination of the bulk FRET efficiency equation 3.2 and the donor brightness before and after acceptor photobleaching, as explained in the text.

Calculated Förster radii and FRET efficiencies

As verification for the obtained bulk FRET efficiencies the Förster radii of a selection of used FRET pairs were calculated. Following the requirements discussed in the *Introduction* section, the radii were determined with the following equations.

The spectral overlap integral J is given as

$$J(\lambda) = \int \overline{f_{\mathrm{D}}}(\lambda)\epsilon_{\mathrm{A}}(\lambda)\lambda^4 d\lambda \tag{3.3}$$

where $\overline{f_{\mathrm{D}}}(\lambda)$ is the normalized donor emission spectrum, and $\epsilon_{\mathrm{A}}(\lambda)$ is the acceptor molar extinction coefficient.

The Förster radius, depending on the fluorescence quantum yield and the spectral overlap, can be obtained with

$$(R_0)^6 = \frac{9 \cdot \ln(10)}{128(\pi)^5 N_{\mathrm{A}}} \frac{\kappa^2 Q_{\mathrm{D}}}{n^4} J \tag{3.4}$$

Q_{D} is the fluorescence quantum yield of the donor in the absence of the acceptor, κ^2 is the dipole orientation factor, describing the relative orientation in space of the transition moment of the donor and acceptor, n is the refractive index of the medium, N_{A} is Avogadro's number, and J is the spectral overlap integral, introduced in 3.3.

	Quantum yield Q_{D} /%
Alexa Fluor 555	10
Alexa Fluor 488	92
Alexa Fluor 647	33
Atto 655	30

TABLE 3.4: **Quantum yields of the respective fluorophores:** The values were taken from the data sheets of the fluorophores.

Values for Q_{D}, the quantum yields (table 3.4), and the excitation/emission spectra were taken from the respective homepages and data sheets of the manufacturers of the fluorophores.

In table 3.5, the calculated values for the Förster radii are shown. Even though the Förster radii for the Alexa Fluor dyes allow for a larger distance between donor and acceptor, the measured bulk FRET efficiency of Alexa Fluor 488 and Atto 655 yielded higher values (table 3.3).

The FRET efficiency depends on the Förster radius, as given in the following equation:

Förster radii /nm	Alexa Fluor 647	Atto 655
Alexa Fluor 555	5.6022	4.6145
Alexa Fluor 488	6.0136	4.7341

TABLE 3.5: **Calculated Förster radii of the various combinations of used fluorophores**

$$E = \frac{1}{1 + (\frac{r}{R_0})^6} \tag{3.5}$$

By estimating the distance r of the donor and the acceptor with r = 4.1 nm, the FRET efficiency can be calculated [24]. The obtained values are given in table 3.6. As expected, the Alexa dye combinations yielded the highest efficiencies.

FRET efficiency	Alexa fluor 647	Atto 655
Alexa Fluor 555	86.68%	67.02%
Alexa Fluor 488	90.87%	70.33%

TABLE 3.6: **Calculated FRET efficiency of the various combinations of applied fluorophores:** The estimated distance between donor and acceptor was r = 4.1 nm [24].

3.2 Diffusion analysis, immobilization and single molecule FRET to decipher TCR:pMHC interactions

Determination of diffusion constants and immobilizations of different peptides presented by MHC complexes and cholesterol beneath and adjacent to the T cell, dwell time of the immobilization of the various pMHC molecules and cholesterol, and, furthermore, the correlation of the duration of these immobilizations with single molecule FRET events between the T cell receptor and its ligand, the pMHC, were the main objectives of this thesis.

In all following experiments, pMHC, ICAM-1 and B7-1 were embedded in supported lipid bilayer (see protocol in the *Materials and Methods* section) to achieve either activating or non-activating conditions, as determined in the previous measurements. The density of the labeled pMHC complexes (figure 3.8, B) allowed for localizing and tracking of single molecule signals, thereby determining diffusion constants and immobilizations of pMHC. The peptides presented by the MHC complex, the latter anchored via His-tags to the supported lipid bilayer, included moth cytochrome c (MCC), β2m and T102S. MCC (88–103, ANERADLIAYLKQATK) is a strong agonist

[24]. T102S is a peptide with a modified amino acid sequence (ANERADLIAYLKQA**S**KGGdSdC), having Threonine substituted by Serine at the position 102 of the amino acid sequence, and is, thereby, supposed to have a weaker binding affinity to the TCR than the MCC peptide. β2m is a Null-peptide - an endogenous self peptide [2] - and shows a completely different amino acid sequence (dHdPdPdHdIdEIQMLKNGKKIPGGdSdC). As a negative control, trace amounts of a cholesterol analogue with a PEG linker and an attached fluorophore KK114 were embedded in the artificial cell membrane and allowed for localizing and tracking of the single molecule signals as well. In general, no interaction of the fluorescent cholesterol analogue with T cells was expected.

The T lymphocytes (figure 3.8, A) were labeled in saturation with single chain fragments (60-70 scFv/μm^2) to increase the probability of observing a single molecule FRET event. The single chain fragments carried the fluorophore Alexa Fluor 488 on the proximal site to the pMHC, J1 (figure 1.9, [24]).

Upon exchanging PBS to HBSS with 1% ovalbumine, 5µl of the T cell suspension was added to the well. Under non-activating conditions, measurements were started upon cell adhesion. The observation of microcluster and cSMAC after cell adhesion triggered the start of measurements under activating conditions. An illumination protocol, described in the *Materials and Methods* section (figure 2.2), was used to take alternating images of fluorescently labeled pMHC single molecule signals in the bilayer (figure 3.8, B), cells (figure 3.8, A) and single molecule FRET events in the acceptor channel upon donor excitation (figure 3.8, C).

This illumination protocol was repeated 200 times, yielding a duration of 6 s per measurement, to ensure the acquisition of data allowing for detection of immobilizations.

The first analysis of this data included the localization and tracking of the single molecule signals of the respective peptides presented by the MHC and cholesterol. Further analysis of this data, determination of diffusion constants and immobilizations, is described in the following sections.

3.2.1 Comparison of diffusion constants beneath and adjacent to T cells in activating and non-activating conditions

First, the interaction between the T cell receptor and the pMHC was probed by observing the diffusion constant of pMHC MCC, T102S, β2m and cholesterol.

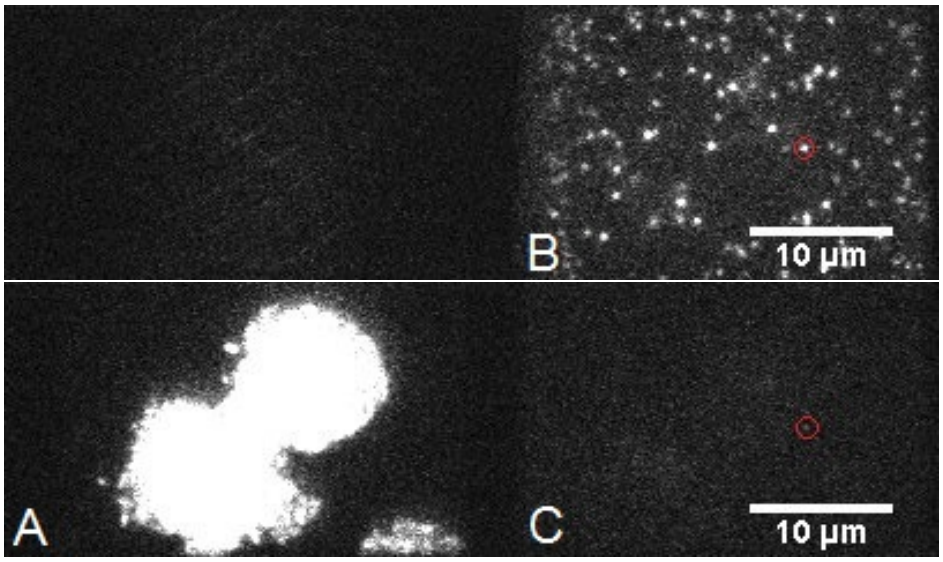

FIGURE 3.8: **single molecule FRET signal:** T cells adhered to a supported lipid bilayer containing ICAM-1, B7-1 and a low density of labeled pMHC Atto 655. A T cell labeled with single chain fragment carrying an Alexa Fluor 488 fluorophore (A) shows interaction with the pMHC (B) indicated by a single molecule FRET event (C).
The images have the same brightness and contrast.

In order to analyze diffusion constants under the cell with respect to the diffusion constant next to the cell, images of stained T cells (figure 3.8, A) were thresholded. A cell mask was generated by setting all values above the threshold to 1, and below the threshold to 0. By projecting this mask into the pMHC channel trajectories beneath, *in*, and adjacent to, *out*, the T cell could be distinguished. The results of diffusion analysis are shown in table 3.7.

The most significant effect was observed under activating conditions with the MCC peptide - the diffusion constant in the interface of the T lymphocyte and the supported lipid bilayer was decreased by 42.59% compared to the diffusion constant adjacent to the T cell. For non-activating conditions the average mobility beneath the T cell yielded a reduction by 38.46%. As expected, the diffusion constants of the null peptide β2m and the modified peptide T102S were not as pronounced influenced as the strong agonistic peptide MCC.

For the negative control, no reduction of the average mobility was expected. However, the data concerning cholesterol showed a decrease of the diffusion constant beneath the cell by 11.19% under activating and by 7.63% under non-activating conditions. Considering the close contact zone between the T cell and the bilayer, the retardation of cholesterol may be explained by interactions of the bulky PEG linker - used to attach the fluorophore to the cholesterol - with T cell molecules.

Diffusion constants [$\mu m^2/s$]					
peptide		activating	% retardation	non-activating	% retardation
MCC	in	0.434	42.59%	0.24	38.46%
	out	0.756		0.39	
β2m	in	0.319	29.11%	0.451	26.19%
	out	0.45		0.611	
T102S	in	0.294	24.22%	0.339	27.71%
	out	0.388		0.469	
Cholesterol	in	1.19	11.19%	1.21	7.63%
	out	1.34		1.31	

TABLE 3.7: **Diffusion constants of pMHC MCC, T102S, β2m and cholesterol:** For each peptide in the MHC complex and cholesterol diffusion constants beneath, *in*, and adjacent, *out*, were determined to quantify the reduction upon presence of the T cell. "activating" indicates 100 unlabeled pMHC MCC molecules/μm^2 and trace amounts of the respective labeled probe anchored to the supported lipid bilayer, whereas "non-activating" conditions include only the trace amounts of the respective labeled probe embedded in the artificial cell membrane.

These data suggest that the average mobilities of the peptides MCC, β2m and T102S presented by MHC are reduced by transiently binding to the T cell receptor. Whether the reduction of the diffusion constants was caused by transient immobilizations, was part of the following analysis.

3.2.2 Immobilisation analysis

Analysis of the trajectories of the pMHC MCC, T102S, β2m and cholesterol included the investigation of immobilizations in the respective trajectory. To be accounted as an immobilization, the steps of a trajectory of the respective probe had to remain in a given radius (r = 1 pixel) for a minimum of 5 steps. Furthermore, the dwell times of the immobilizations were determined by multiplying the number of consecutive frames in which the immobilization is detected with the time lag of 30 ms. Table 3.8 shows the dwell times of immobilizations and the percentage of trajectories containing immobilizations. The percentage of immobilized trajectories, $IT_{\%}$, is given by

$$\mathrm{IT}_{\%} = \frac{N_{\mathrm{immob}}}{\mathrm{T}} \tag{3.6}$$

where N_{immob} is the number of immobilized trajectories and T is total number of trajectories.

Dwell times of immobilizations [ms]					
peptide		activating	$IT_{\%}$	non-activating	$IT_{\%}$
MCC	in	249.44	13.1 %	390.23	31.31%
	out	191.81	2.3%	187.44	5.36%
β2m	in	245.72	17.11%	298.97	11.7%
	out	199.2	4.3%	263.64	3.1%
T102S	in	223.1	17.06%	322.65	20.3%
	out	143.55	5.8%	249.81	3.41%
Cholesterol	in	354.22	8.19%	256.37	3.8%
	out	256.06	1.79%	197.24	1.4%

TABLE 3.8: **Dwell times of immobilizations of pMHC MCC, T102S, β2m and cholesterol:** For each peptide and cholesterol dwell times of the immobilization beneath, *in*, and adjacent to the T cell, *out*, were determined. $IT_{\%}$ is the percentage of the number of immobilized trajectories relative to the total number of trajectories. "activating" indicates 100 unlabeled pMHC MCC molecules/μm^2 and trace amounts of the respective labeled probe anchored to the supported lipid bilayer, whereas "non-activating" conditions included only the trace amounts of the respective labeled probe embedded in the artificial cell membrane.

Interestingly, the highest amount of immobilizations, 31.31%, was observed under non-activating conditions with the MCC peptide in the pMHC complex. The dwell time yielded approximately 390 ms beneath the T cell. This effect was not as pronounced as under activating conditions.

Analysis of the null peptide β2m and modified peptide T102S under activating conditions beneath the cell yielded dwell times of 245 ms and 223 ms, respectively, and the percentage of immobilizations were comparable, both approximately 17%. However, under non-activating conditions differences between β2m and T102S were observed: dwell times were longer, 298 ms and 322 ms, respectively, and the percentage of immobilized trajectories, $IT_{\%}$, varied significantly (table 3.8).

The negative control with cholesterol yielded a lower fraction of immobilizations beneath the cell, 8.19% under activating and 3.8% under non-activating conditions, compared to pMHC. This result is in good agreement with the obtained data from the diffusion analysis, also showing negligible reduction of the diffusion constant of cholesterol in the interface of the T cell with the supported lipid bilayer.

At first, the data in table 3.8 contradicts the diffusion constants data shown in table 3.7. However, the direct comparison of the values may not be justified due to different analysis approaches. An immobilization is considered as one individual immobilization if the number of steps assigned to this

immobilization exceeds a minimum of 5 steps. Hence, one long immobilization could reduce the average mobility significantly. Consequently, the fraction of immobilized trajectories must not necessarily correlate with the reduction of the average mobility. Further analysis is required to determine the exact cause of this discrepancy. In the *Analysis considerations* section, several issues of the applied analysis methods are discussed.

3.2.3 single molecule FRET

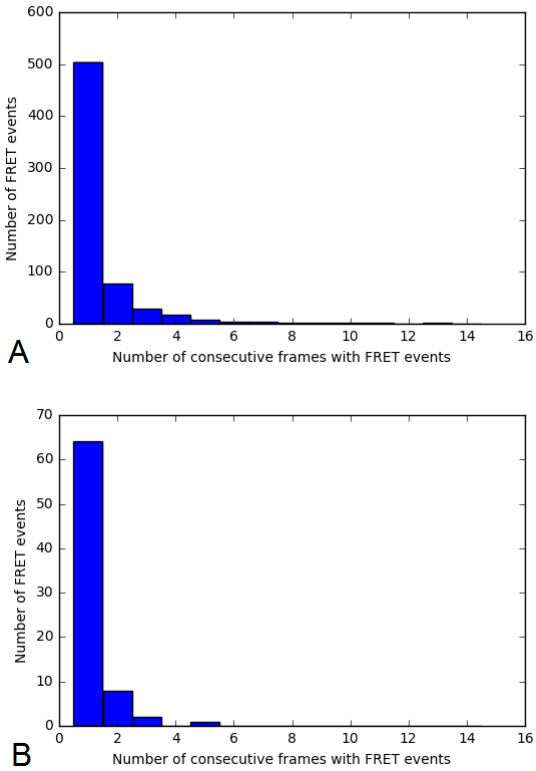

FIGURE 3.9: **Number of consecutive frames with single molecule FRET events:** Most of the FRET events were observable for one frame only.
A: A total of 649 single molecule FRET events were detected under activating conditions (100 unlabeld pMHC molecules/μm^2 and trace amounts, 0.1-1 molecules/μm^2, of pMHC Atto 655).
B: Fewer FRET events, 75, were measured in non activating conditions (approximately 0.1-1 pMHC Atto 655 molecules/μm^2).

Single molecule FRET events indicate the direct interaction of TCR:pMHC. Therefore, it was of special interest to determine the number and average duration of single molecule FRET events. With *Coloc*, a program described in the *Materials and Methods* section which is capable of colocalizing signals in different images, single molecule FRET events (3.8, C) and the respective pMHC signals were detected. Average values of single molecule FRET

durations were determined by multiplication of the number of frames with detected single molecule FRET events with the time lag of 30 ms.

Among 23 cells 649 single molecule FRET events were observed under activating conditions. A high fraction of the single molecule FRET events in activating conditions was detected in one frame only (figure 3.9, A). The average duration of the single molecule FRET events was 53.2 ms under activating conditions.

In figure 3.9, B, the result for the analysis of the single molecule FRET events under non-activating conditions is shown. 75 single molecule FRET events were observed among 27 cells. Comparably to the activating conditions, a high fraction of the single molecule FRET events was observable for one frame. On average single molecule FRET durations were observed for 37.1 ms under non-activating conditions.

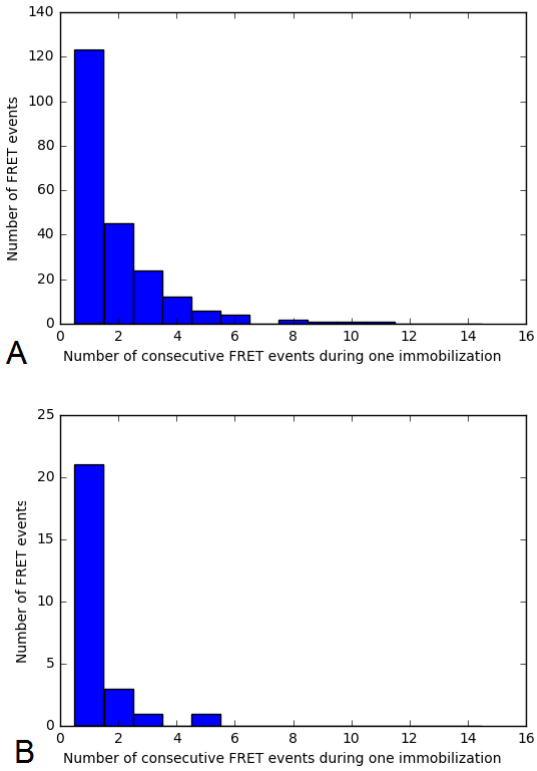

FIGURE 3.10: **Number of consecutive FRET events during one immobilization:**
A: 5024 immobilized trajectories included 146 single molecule FRET events activating conditions (100 unlabeled pMHC molecules/μm^2 and 0.1-1 pMHC Atto 655 molecules/μm^2).
B: 6301 immobilized trajectories including 27 single molecule FRET events were analysed in non-activating conditions (0.1-1 pMHC Atto 655 molecules/μm^2).

3.2.4 Correlation of immobilizations and single molecule FRET

An immobilization does not allow for direct observation of molecular interaction kinetics between TCR:pMHC due to lacking evidence of direct interaction. To determine, whether an immobilization included the engagement of TCR:pMHC, the immobilized trajectories were analyzed with *Coloc* to detect single molecule FRET events in the respective trajectory. Single molecule FRET events indicate a direct interaction of TCR:pMHC.

The search for single molecule FRET events within immobilized trajectories under activating conditions yielded 146 single molecule FRET events compared to a total number of 5024 immobilizations (figure 3.10, A). Under non-activating conditions 27 single molecule FRET events were detected in a total of 6301 immobilizations (figure 3.10, B). This result suggests that not every immobilization is caused by a binding event to the TCR.

Chapter 4

Discussion

4.1 Diffusion analysis

Of special interest with regard to the single molecule tracking experiments was to evaluate, whether the pMHC molecules beneath the cell exhibit a lower diffusion constant compared to the pMHC molecules adjacent to the interface of cell and bilayer.

A reduction of the diffusion constant beneath the T cell was expected in case of supported lipid bilayers containing pMHC for all different peptides (table 3.7). Indeed, a significant decrease of the average mobility was measured for the MCC peptide. Taking the lower binding affinities of the endogenous self-peptide β2m and the modified peptide T102S into account [24], the results obtained for their reduction of the diffusion constants is reasonable as the decrease is not as significant as observed for the MCC peptide. Thus, it is attractive to speculate that the reduction of the average mobility is caused by the transient binding of the peptide MHC to the TCR.

Axmann et al. [2] observed a comparable diffusion constant for pMHC MCC. However, in this thesis a significant decrease of the diffusion constant of the endogenous self-peptide β2m and the modified peptide T102S beneath the T cell was observed, whereas, in the studies of Axmann et al. [2] no reduction of the average mobility was measured for these peptides. In addition, Axmann et al. [2] estimated an interaction duration of 150 ms. This finding is not in agreement with the determined dwell times of immobilizations and the durations of single molecule FRET events in this thesis, yielding 250 ms and 53 ms, respectively, for pMHC MCC in activating conditions. However, the studies of Axmann et al. [2] were recorded under physiological conditions, whereas the data presented in this thesis was obtained at room temperature. Therefore, the comparison of absolute values is not justified.

Furthermore, this thesis compared the obtained diffusion data with a negative control, cholesterol, showing a low level of reduction of the diffusion constant in general.

Unexpectedly, the diffusion constants adjacent to the T cell did not yield the same absolute values, upon comparison of activating and non-activating conditions or among different pMHCs. The temperature (22°C), imaging buffer (HBSS + 1% ovalbumine) and illumination protocol were exactly the same for all measurements. Under these conditions, it is reasonable to assume comparable absolute values of the diffusion constants of the pMHCs adjacent to the T cell. Indeed, this was observed in case of cholesterol, but not for the various pMHCs. The difference between the diffusion constants outside the T cell - supported lipid bilayer interface differed up to 52% in case of the MCC. Consequently, the absolute values were not comparable and the ratio of the diffusion constant beneath and adjacent to the T cell was calculated to obtain comparable values.

4.2 Immobilizations

The obtained data on dwell times of immobilizations of the pMHCs and cholesterol offer a different point of view for the interaction dynamics of pMHC complexes with the TCR. O'Donoghue et al. [19] claim to observe direct interactions of single molecules of the pMHC with the TCR by the analysis of immobilizations of single pMHC molecules. Their data suggest interaction durations of approximately 5 s. However, the applied illumination time of 500 ms does not allow for observation of interactions shorter than the illumination time. Moreover, they do not provide evidence that one observed immobilized pMHC molecule is indeed one single pMHC complex interacting with the TCR. Stating that this method is capable of detecting molecular interaction kinetics on the single molecule level may not be justified.

The results of this thesis suggest dwell times of immobilizations in the range of several 100 ms. However, data obtained by immobilization analysis does not allow for extracting interaction times of the pMHC with the TCR due to lacking evidence of engagement of the two molecules.

4.2.1 Analysis considerations

Several possible issues can influence the results obtained by the used algorithm. One limitation of the used program includes the lack of detecting gaps. Consequently, if pMHC signals are not observed for one frame due

to blinking, the algorithm would identify these signals as two separate immobilizations, leading to shorter dwell times. Thereby, one long immobilization is split into two shorter ones. On the contrary, by allowing for gaps, two individual immobilizations could be incorrectly associated as one immobilization. Hence, the dwell times would be longer.

Another consideration comprises the arbitrary selection of the allowed radius, in which the steps have to remain to be assigned to an immobilization (figure 4.1). This problem is comparable to the issue with the previously discussed gaps. If the chosen radius is too large, signals, which do not belong to the identical immobilization, are incorrectly assigned to this immobilization. On the contrary, a radius, which is too small, is not capable of detecting immobilized signals. Bleaching could as well reduce the dwell time of the immobilizations.

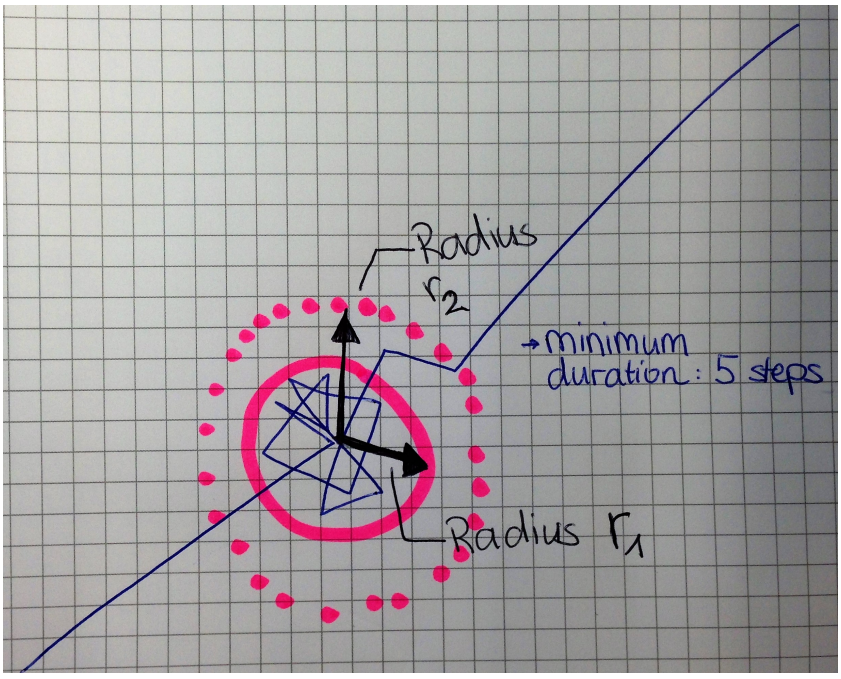

FIGURE 4.1: **Considerations of chosen radii:** Depending on the size of the arbitrarily chosen radius, the algorithm determines different dwell times of immobilizations. The dwell time in case of chosen r_1 is shorter than for radius r_2.

The minimum amount of steps is another arbitrarily chosen, but yet decisive parameter. With this number the lower limit of the length of one trajectory is defined. Thereby, a minimum dwell time is set and shorter immobilizations are not detected as true immoblizations. This parameter influences the analysis of the correlation of single molecule FRET events with immobilizations since shorter immobilization are not considered and the thereby occurring single molecule FRET events are neglected.

4.2.2 Comparison of immobilizations beneath and adjacent to the T cell

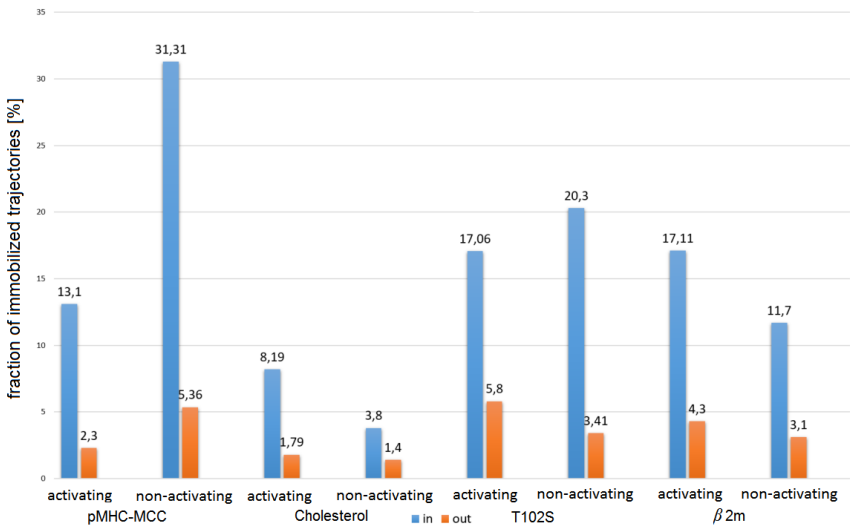

FIGURE 4.2: **Fractions of immobilized trajectories:** Summary of the ratio of immobilized trajectories and the total number of trajectories, of the various peptides and cholesterol *in*, beneath the T cell, and *out*, adjacent to the T cell. Activating, 100 unlabeled pMHC MCC molecules/μm^2 and trace amounts of the respective peptide or cholesterol anchored to the supported lipid bilayer, and non-activating, only trace amounts of the respective peptide or cholsterol (0.1-1 molecule/μm^2) embedded in the artificial cell membrane, conditions are compared.

Figure 4.2 shows the ratios of immobilized trajectories and the total number of trajectories beneath, *in*, or adjacent to, *out*, the T cell - supported lipid bilayer interface.

As expected, a higher fraction of trajectories is immobilized beneath the T cell compared to the area adjacent to the T cell. This indicates interaction of the T lymphocyte with the respective molecule. The fractions of immobilized trajectories adjacent to the T lymphocyte were significantly lower and yielded values between 1.4 and 5.8%.

pMHC MCC (figure 4.2) shows an interesting behavior: the fraction of immobilized trajectories beneath the T lymphocyte in activating conditions is lower compared to the fraction of immobilized trajectories in non-activating conditions. These data suggest a competition of the labeled pMHC proteins with the unlabeled pMHC molecules. In activating conditions a high number of pMHC molecules is present, which compete for binding to the T cell receptor. Thus, not all pMHC binding events to the T cell receptor are observed, yielding a lower fraction of obtained immobilizations. In non-activating conditions fewer pMHC molecules are present - the probability

of observing all of the pMHC:TCR interactions is higher.

As expected, the modified peptides T102S and the endogenous self-peptide β2m (figure 4.2) yielded lower fractions of immobilizations beneath the T cell compared to the conventional triggering peptide MCC.

For cholesterol (figure 4.2), the analysis yielded lower fractions of immobilizations. However, immobilizations are more frequent beneath T cells, thereby supporting the conclusion from diffusion analysis, that the close proximity of T cell and supported lipid bilayer causes interactions with cholesterol and the T cell.

4.3 single molecule FRET

The measurements yielded a significant difference of the amount of single molecule FRET events in activating and non activating conditions with pMHC MCC. In activating conditions 649 single molecule FRET events (figure 3.9, A) were observed, whereas non-activating conditions yielded 75 single molecule FRET events (figure 3.9, B). Note, that a competition as observed in immobilization analysis was not detected. This discrepancy is discussed in the next section. The number of measured cells was comparable: in activating conditions 23 cells and in non activating conditions 27 cells were analyzed on a supported lipid bilayer containing pMHC MCC. By monitoring the duration of single molecule FRET events, an interaction duration of 53.2 ms, in activating, and 37.1 ms, in non activating conditions, was determined. This method is suitable for observing direct interactions between the TCR and pMHC. In contrast to immobilization analysis, single molecule FRET allows a direct observation of the interaction.

The low values for interaction duration in this thesis is in contrast to the interaction duration of pMHC MCC:TCR in the literature. Axmann et al. [2] and Huppa et al. [24] observed interaction durations of 150 ms, whereas O'Donoghue et al. [19] claim to measure interaction durations in the range of seconds. The single molecule FRET events measured in this thesis were obtained at room temperature, whereas the interaction durations in the mentioned publications were determined at physiological temperatures (37°C). At room temperature, Huppa et al. [24] showed that these processes are slower than at physiological temperatures (1.68 s), whereas O'Donoghue et al. [19] did not observe a significant difference of the interaction duration at physiological temperature. However, the data is not corrected for bleaching, which may cause shorter single molecule FRET durations due to photobleaching.

4.4 Correlation of single molecule FRET and dwell time of immobilizations

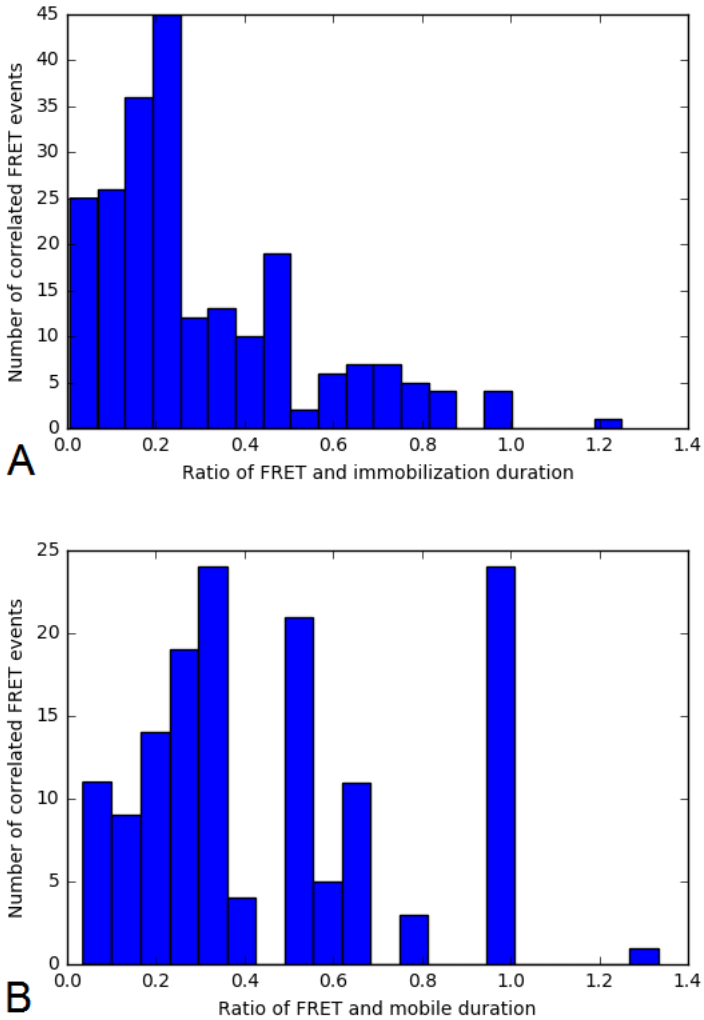

FIGURE 4.3: **Histogram of ratios between single molecule FRET durations and the durations of immobilized (A) or mobile (B) trajectories:** In immobile trajectories, the analysis showed that the duration of single molecule FRET events was shorter than the respective immobilization *A*. Moreover, more correlated single molecule FRET events were found in immobilized trajectories compared to mobile trajcetories *B*. These data were obtained on a supported lipid bilayer with activating conditions (100 pMHC MCC molecules/μm^2).

Since an immobilization does not allow for direct observation of molecular interaction kinetics between TCR:pMHC due to lacking evidence of direct interaction, the correlation between the number and duration of single molecule FRET events and the duration of immobilizations was required.

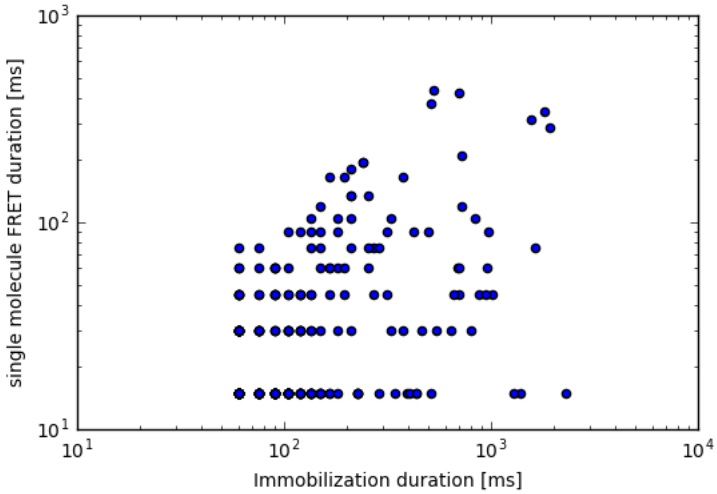

FIGURE 4.4: **Correlation of single molecule FRET event duration with the duration of immobilized trajectories:** No significant correlation between the duration of single molecule FRET events and immobilized trajectories could be determined. These data were obtained on a supported lipid bilayer with activating conditions (100 pMHC MCC molecules/μm^2).

High numbers of immobilized trajectories could be correlated with few single molecule FRET events. For activating conditions (figure 3.10, A), 5024 immobilized trajectories showed 146 single molecule FRET events, whereas in non-acitvating conditions (figure 3.10, B) 6301 analyzed immobilized trajectories included 27 single molecule FRET events. Consequently, not every immobilization included a single molecule FRET event, the latter indicating the direct interaction of TCR:pMHC.

A further analysis included the correlation between immobilization durations and duration of single molecule FRET events within the respective trajectory in activating conditions. However, the analysis method only allows for immobilizations longer than 5 steps, consequently, shorter trajectories including single molecule FRET events, are not considered. The analysis yielded that the duration of the dwell time exceeds the duration of the single molecule FRET event (figure 4.3). In case of the duration of immobilized trajectories a pronounced accumulation of single molecule FRET events, lasting 20% of the immobilization duration, was observed (figure 4.3, A). On the contrary, fewer single molecule FRET events could be correlated with mobile trajectories, an indication for single molecule FRET events rather occuring during immobilizations (figure 4.3, B).

However, no significant correlation between the duration of single molecule FRET events and the duration of immobilizations could be observed (figure 4.4). The correlation coefficient yielded 0.43.

Due to the finding that immobilizations of pMHC are detected more frequently than single molecule FRET events, other processes beside the interaction of pMHC with the TCR are suspected to cause the immobilizations of the pMHC. Possible mechanisms comprise interaction with another receptor on the T cell surface, steric hindrance or undetected interactions with the TCR. CD4 is a receptor of the T cell, which is interacting with another site of pMHC [29], and could thereby cause retardation or immobilization of pMHC complexes. Bulkiness of the pMHC could as well be a reason to reduce the average mobility in the T cell - pMHC interface due to the close contact zone. Another aspect comprises the stability of the anchoring of the single chain fragment to the TCR. If the single chain fragment detaches, not every interaction between the TCR and pMHC can be detected resulting in fewer observed single molecule FRET events.

This result suggests further investigation of the cause of the immobilizations.

Chapter 5

Outlook

The data presented in this thesis suggest various follow-up experiments and further controls.

5.1 Further investigations of imaging buffers

An unsolved issue remained due to the differences in the diffusion constants adjacent to the T lymphocyte. Considering the wide spread of the diffusion constants, it is attractive to speculate that the ovalbumine causes other problems. Therefore, new controls are required to obtain a deeper knowledge about the properties of ovalbumine and its effect on a supported lipid bilayer. Furthermore, experiments, attempting to determine the necessity of FCS/ovalbumine, are of interest. Maybe, T cells show the same behavior in pure HBSS and the added FCS/ovalbumine do not affect T cell function. Addition of FCS or ovalbumine saturates potential binding sites of the artificial cell membrane and is supposed to prevent unwanted T cell activation. To verify this consideration, control experiments of T cells on non-activating artificial lipid membranes in pure HBSS are required to test, whether T cells are activated due to the missing components.

5.2 Elevated temperatures

Of special interest would be the observation of diffusion constants, immobilizations and single molecule FRET events at physiological temperature (37°C). It is attractive to assume elevated diffusion constants, shorter immobilizations and single molecule FRET events at physiological temperature (37°C) compared to room temperature (22°C). The correlation between these data would be interesting. Furthermore, experiments at elevated temperatures, 41 or 42°C, would surrogate an environment imitating fever, revealing the interaction kinetics of the T cell receptor with its ligand, the peptide MHC, under these conditions.

List of Figures

List of Tables

Bibliography

[1] Sanford M. Simon Alexa L. Mattheyses and Joshua Z. Rappoport. "Imaging with total internal reflection fluorescence microscopy for the cell biologist". In: *Journal of Cell Science* 123 (2010). DOI: 10.1242/jcs.

[2] M. Axmann et al. "Determination of interaction kinetics between the T cell receptor and peptide-loaded MHC class II via single-molecule diffusion measurements". In: *Biophys J* 103.2 (2012), pp. L17–9. ISSN: 1542-0086 (Electronic) 0006-3495 (Linking). DOI: 10.1016/j.bpj.2012.06.019. URL: http://www.ncbi.nlm.nih.gov/pubmed/22853916.

[3] Daniela Bovenkamp. "Austauschkinetik von pMHC in TCR Clustern". In: (2015).

[4] M. Brameshuber and G. J. Schütz. "Single Molecule Measurements in Membranes". In: (2012), pp. 337–365. DOI: 10.1016/b978-0-12-374920-8.00527-0.

[5] J. G. Burchfield et al. "Exocytotic vesicle behaviour assessed by total internal reflection fluorescence microscopy". In: *Traffic* 11.4 (2010), pp. 429–39. ISSN: 1600-0854 (Electronic) 1398-9219 (Linking). DOI: 10.1111/j.1600-0854.2010.01039.x. URL: https://www.ncbi.nlm.nih.gov/pubmed/20070611.

[6] J C Cambier. "Antigen and Fc Receptor Signaling. The awesome power of the Immunoreceptor Tyrosine-Based Activation Motif (ITAM)". In: *The Jounal of Immunology* 155 (1995), pp. 3281–3285.

[7] G. Campi, R. Varma, and M. L. Dustin. "Actin and agonist MHC-peptide complex-dependent T cell receptor microclusters as scaffolds for signaling". In: *J Exp Med* 202.8 (2005), pp. 1031–6. ISSN: 0022-1007 (Print) 0022-1007 (Linking). DOI: 10.1084/jem.20051182. URL: http://www.ncbi.nlm.nih.gov/pubmed/16216891.

[8] A. K. Chakraborty and A. Weiss. "Insights into the initiation of TCR signaling". In: *Nat Immunol* 15.9 (2014), pp. 798–807. ISSN: 1529-2916 (Electronic) 1529-2908 (Linking). DOI: 10.1038/ni.2940. URL: http://www.ncbi.nlm.nih.gov/pubmed/25137454.

[9] V. T. Chang et al. "Initiation of T cell signaling by CD45 segregation at 'close contacts'". In: *Nat Immunol* 17.5 (2016), pp. 574–82. ISSN: 1529-2916 (Electronic) 1529-2908 (Linking). DOI: 10.1038/ni.3392. URL: http://www.ncbi.nlm.nih.gov/pubmed/26998761.

[10] K. Choudhuri et al. "Polarized release of T-cell-receptor-enriched microvesicles at the immunological synapse". In: *Nature* 507.7490 (2014), pp. 118–23. ISSN: 1476-4687 (Electronic) 0028-0836 (Linking). DOI: 10.1038/nature12951. URL: http://www.ncbi.nlm.nih.gov/pubmed/24487619.

[11] Robert M. Clegg. "Chapter 1 Förster resonance energy transfer—FRET what is it, why do it, and how it's done". In: 33 (2009), pp. 1–57. ISSN: 00757535. DOI: 10.1016/s0075-7535(08)00001-6.

[12] Darrell J. Irvine Mark M. Davis. "Direct observation of ligand recognition by T cells". In: *Nature* 419 (2002).

[13] S. J. Davis and P. A. van der Merwe. "The kinetic-segregation model: TCR triggering and beyond". In: *Nat Immunol* 7.8 (2006), pp. 803–9. ISSN: 1529-2908 (Print) 1529-2908 (Linking). DOI: 10.1038/ni1369. URL: http://www.ncbi.nlm.nih.gov/pubmed/16855606.

[14] M. L. Dustin. "The Immunological Synapse". In: *Cancer Immunology Research* 2.11 (2014), pp. 1023–1033. ISSN: 2326-6066 2326-6074. DOI: 10.1158/2326-6066.cir-14-0161.

[15] Shannon K. Bromley Michael L. Dustin. "The immunological Synapse". In: *Annu Rev Immunol* 19 (2001), pp. 375–396.

[16] Yuri Sykulev Herman N. Eisen. "Evidence that a Single Peptide–MHC Complex on a Target Cell Can Elicit a Cytolytic T Cell Response". In: *Immunity* 4 (1996), pp. 565–571.

[17] B. A. Freiberg et al. "Staging and resetting T cell activation in SMACs". In: *Nat Immunol* 3.10 (2002), pp. 911–7. ISSN: 1529-2908 (Print) 1529-2908 (Linking). DOI: 10.1038/ni836. URL: http://www.ncbi.nlm.nih.gov/pubmed/12244310.

[18] H. Schindler G. J. Schuitz and Th. Schmidt. "Single-Molecule Microscopy on Model Membranes Reveals Anomalous Diffusion". In: *Biophysical Journal* 73 (1997), pp. 1073–1080.

[19] Jay T. Groves Geoff P O'Donoghue Jenny J Lin. "Direct single molecule measurement of TCR triggering by agonist pMHC in living primary T cells". In: *eLIFE* (2013). DOI: 10.7554/eLife.00778.00110.7554/eLife.00778.002.

[20] Sungchul Hohng Ha and Taekjip. "Single-Molecule FRET". In: *Molecular Imaging*. Oxford University Press, 2005.

[21] N. C. Hartman, J. A. Nye, and J. T. Groves. "Cluster size regulates protein sorting in the immunological synapse". In: *Proc Natl Acad Sci*

U S A 106.31 (2009), pp. 12729–34. ISSN: 1091-6490 (Electronic) 0027-8424 (Linking). DOI: 10.1073/pnas.0902621106. URL: http://www.ncbi.nlm.nih.gov/pubmed/19622735.

[22] J. Huang et al. "The kinetics of two-dimensional TCR and pMHC interactions determine T-cell responsiveness". In: *Nature* 464.7290 (2010), pp. 932–6. ISSN: 1476-4687 (Electronic) 0028-0836 (Linking). DOI: 10.1038/nature08944. URL: http://www.ncbi.nlm.nih.gov/pubmed/20357766.

[23] J. B. Huppa and M. M. Davis. "T-cell-antigen recognition and the immunological synapse". In: *Nat Rev Immunol* 3.12 (2003), pp. 973–83. ISSN: 1474-1733 (Print) 1474-1733 (Linking). DOI: 10.1038/nri1245. URL: https://www.ncbi.nlm.nih.gov/pubmed/14647479.

[24] J. B. Huppa et al. "TCR-peptide-MHC interactions in situ show accelerated kinetics and increased affinity". In: *Nature* 463.7283 (2010), pp. 963–7. ISSN: 1476-4687 (Electronic) 0028-0836 (Linking). DOI: 10.1038/nature08746. URL: http://www.ncbi.nlm.nih.gov/pubmed/20164930.

[25] George F. Gao Jakobsen and Bent K. "Molecular interactions of coreceptor CD8 and MHC class I: the molecular basis for functional coordination with the T-cell receptor". In: *Immunology today* 21.12 (2000).

[26] J. R. James and R. D. Vale. "Biophysical mechanism of T-cell receptor triggering in a reconstituted system". In: *Nature* 487.7405 (2012), pp. 64–9. ISSN: 1476-4687 (Electronic) 0028-0836 (Linking). DOI: 10.1038/nature11220. URL: http://www.ncbi.nlm.nih.gov/pubmed/22763440.

[27] Y. Kaizuka et al. "Mechanisms for segregating T cell receptor and adhesion molecules during immunological synapse formation in Jurkat T cells". In: *Proc Natl Acad Sci U S A* 104.51 (2007), pp. 20296–301. ISSN: 1091-6490 (Electronic) 0027-8424 (Linking). DOI: 10.1073/pnas.0710258105. URL: http://www.ncbi.nlm.nih.gov/pubmed/18077330.

[28] Itamar Kass, Ashley M. Buckle, and Natalie A. Borg. "Understanding the structural dynamics of TCR-pMHC interactions". In: *Trends in Immunology* 35.12 (2014), pp. 604–612. ISSN: 14714906. DOI: 10.1016/j.it.2014.10.005.

[29] Q. J. Li et al. "CD4 enhances T cell sensitivity to antigen by coordinating Lck accumulation at the immunological synapse". In: *Nat Immunol* 5.8 (2004), pp. 791–9. ISSN: 1529-2908 (Print) 1529-2908 (Linking). DOI: 10.1038/ni1095. URL: https://www.ncbi.nlm.nih.gov/pubmed/15247914.

[30] F.R.S. Lord Rayleigh. "Investigations in Optics, with special reference to the Spectroscope". In: *Philosophical Magazine and Journal of Science* 8 (1879).

[31] P. Anton van der Merwe. "The TCR Triggering Puzzle". In: *Immunity* 14 (2001), pp. 665 –668.

[32] S. Minguet and W. W. Schamel. "A permissive geometry model for TCR-CD3 activation". In: *Trends Biochem Sci* 33.2 (2008), pp. 51–7. ISSN: 0968-0004 (Print) 0968-0004 (Linking). DOI: 10.1016/j.tibs.2007.10.008. URL: http://www.ncbi.nlm.nih.gov/pubmed/18201888.

[33] Douglas Murphy. *Fundamentals of Light Microscopy and Electronic Imaging*. Wiley-Liss, 2001.

[34] Kenneth Murphy. *Janeway's Immunobiology*. 8th ed. Garland Science, Taylor and Francis Group, 2012.

[35] P S Linsley A Aruffo N K Damle K Klussman and J A Ledbetter. "Differential regulatory effects of intercellular adhesion molecule-1 on costimulation by the CD28 counter-receptor B7". In: *The Jounal of Immunology* 149 (1992), pp. 2541–2548.

[36] Jeffrey A. Nye and Jay T. Groves. "Kinetic Control of Histidine-Tagged Protein Surface Density on Supported Lipid Bilayers". In: *Langmuir* 24 (2008).

[37] Gerhard Schütz. "Microscopy of Biomolecules". In: (2014).

[38] Timothy A. Springer. "Adhesion receptors of the immune system". In: *Nature* 346 (1990).

[39] Alain Trautmann. "Microclusters initiate and sustain T cell signaling". In: *Nature Immunology* 6 (2005).

[40] R. Varma et al. "T cell receptor-proximal signals are sustained in peripheral microclusters and terminated in the central supramolecular activation cluster". In: *Immunity* 25.1 (2006), pp. 117–27. ISSN: 1074-7613 (Print) 1074-7613 (Linking). DOI: 10.1016/j.immuni.2006.04.010. URL: http://www.ncbi.nlm.nih.gov/pubmed/16860761.

[41] S. Wieser and G. J. Schutz. "Tracking single molecules in the live cell plasma membrane-Do's and Don't's". In: *Methods* 46.2 (2008), pp. 131–40. ISSN: 1095-9130 (Electronic) 1046-2023 (Linking). DOI: 10.1016/j.ymeth.2008.06.010. URL: http://www.ncbi.nlm.nih.gov/pubmed/18634880.

[42] MD William E. Paul. *Fundamental Immunology*. 7th ed. Lippincott Williams and Wilkins, 2013.

[43] Matthew E Call Kai Wucherpfennig. "The Organizing Principle in the Formation of the T Cell Receptor-CD3 Complex". In: *Cell* 111 (2002), 967–979.

[44] A. Yildiz et al. "Myosin V walks hand-over-hand: single fluorophore imaging with 1.5-nm localization". In: *Science* 300.5628 (2003), pp. 2061–5. ISSN: 1095-9203 (Electronic) 0036-8075 (Linking). DOI: 10.1126/science.1084398. URL: https://www.ncbi.nlm.nih.gov/pubmed/12791999.

[45] T. Yokosuka et al. "Newly generated T cell receptor microclusters initiate and sustain T cell activation by recruitment of Zap70 and SLP-76". In: *Nat Immunol* 6.12 (2005), pp. 1253–62. ISSN: 1529-2908 (Print) 1529-2908 (Linking). DOI: 10.1038/ni1272. URL: http://www.ncbi.nlm.nih.gov/pubmed/16273097.

[46] Ignacy Gryczynski Zygmunt Gryczynski and Joseph R. Lakowicz. "Basics of fluorescence and FRET". In: *Molecular Imaging*. Oxford University Press, 2005.